OXFORD GENETICS

GENETICS, 2021, 219(3), iyab139
DOI: 10.1093/genetics/iyab139
Advance Access Publication Date: 28 August 2021
Neurogenetics

UNC-16 alters DLK-1 localization and negatively regulates actin and microtubule dynamics in *Caenorhabditis elegans* regenerating neurons

Sucheta S. Kulkarni,[1] Vidur Sabharwal ,[2] Seema Sheoran ,[1] Atrayee Basu,[3] Kunihiro Matsumoto,[4] Naoki Hisamoto ,[4] Anindya Ghosh-Roy,[3] and Sandhya P. Koushika [2,*]

[1]National Centre for Biological Sciences, Tata Institute of Fundamental Research, Bangalore, 560065, India,
[2]Department of Biological Sciences, Tata Institute of Fundamental Research, Mumbai, Maharashtra 400005, India,
[3]Department of Biotechnology National Brain Research Centre, Manesar 122052, India, and
[4]Department of Molecular Biology, Nagoya University, Nagoya 4648601, Japan

*Corresponding author: Department of Biological Sciences, Tata Institute of Fundamental Research, Homi Bhabha Road, Colaba, Mumbai 400 005, India. Email: spkoushika@tifr.res.in

Abstract

Neuronal regeneration after injury depends on the intrinsic growth potential of neurons. Our study shows that UNC-16, a *Caenorhabditis elegans* JIP3 homolog, inhibits axonal regeneration by regulating initiation and rate of regrowth. This occurs through the inhibition of the regeneration-promoting activity of the long isoform of DLK-1 and independently of the inhibitory short isoform of DLK-1. We show that UNC-16 promotes DLK-1 punctate localization in a concentration-dependent manner limiting the availability of the long isoform of DLK-1 at the cut site, minutes after injury. UNC-16 negatively regulates actin dynamics through DLK-1 and microtubule dynamics partially via DLK-1. We show that post-injury cytoskeletal dynamics in *unc-16* mutants are also partially dependent on CEBP-1. The faster regeneration seen in *unc-16* mutants does not lead to functional recovery. Our data suggest that the inhibitory control by UNC-16 and the short isoform of DLK-1 balances the intrinsic growth-promoting function of the long isoform of DLK-1 *in vivo*. We propose a model where UNC-16's inhibitory role in regeneration occurs through both a tight temporal and spatial control of DLK-1 and cytoskeletal dynamics.

Keywords: JIP3; DLK; UNC-16; actin; microtubules; regeneration; axon; *C. elegans*

Introduction

Neurons in the adult nervous system have a limited ability to regenerate after injury. Studies have shown that the extent of neuronal regeneration depends on the balance between factors that inhibit and promote neuronal regeneration which can be both extrinsic and intrinsic to the injured neuron. An important factor downstream of the injury signaling cascade is the dynamics of cytoskeletal elements (Hur *et al.* 2012; Chisholm 2013; Blanquie and Bradke 2018). After neuronal injury, microtubule dynamics increase under the control of an early injury signaling cascade (Lu *et al.* 2015). It has been shown that regulation of microtubule dynamics and polarity in response to JNK signaling is crucial to initiate regeneration of an injured axon (Stone *et al.* 2010). The regenerating neurons also form new growth cones which are rich in actin, actin filaments and their associated proteins and are together responsible for both formation and motility of the growth cone (Gomez and Letourneau 2014).

The balance between growth-promoting and inhibiting factors determines the extent to which a neuron regenerates. This can be achieved in multiple ways, for instance several kinases have been reported to regulate the intrinsic growth potential of regenerating neurons such as, Protein Kinase C (Lee *et al.* 2013), S6 Kinase (Hubert *et al.* 2014), MAP Kinases such as Erk (Hanz *et al.* 2003), JNK (Lindwall and Kanje 2005), and Dual Leucine zipper Kinase (DLK) (Hammarlund *et al.* 2009). Scaffolding molecules can regulate the activity of such kinases in a spatio-temporal manner. In addition, they can bring together several proteins serving to modulate entire signaling cascades. JIPs are a family of classical scaffolding molecules known to be able to switch their roles from growth-promoting to growth-inhibiting based on their levels, extent, and duration of activity (Whitmarsh 2006).

JIP3, a JNK-interacting protein (JIP) family member, assists in the formation of a functional JNK signaling module by assembling specific components of the MAPK cascade which are known to modulate neuronal growth in various systems (Ito *et al.* 1999; Kelkar *et al.* 2000; Byrd *et al.* 2001). JIP3 interacts with the specific kinases of the JNK signaling pathway *i.e.*, JNK, MKK7, and MLK3 (Whitmarsh, Cavanagh *et al.* 1998). MAPKKKs are the most upstream kinases in the MAPK cascade and play a role in regulating signal specificity (Kyriakis and Avruch 2012). DLK, an MAPKKK,

Received: July 09, 2021. **Accepted:** August 13, 2021

regulates synapse formation and is essential for neuronal regeneration (Nakata *et al.* 2005; Hammarlund *et al.* 2009). DLK-1 activation is tightly regulated and occurs only in the presence of specific stimuli such as neuronal injury (Nakata *et al.* 2005; Yan and Jin 2012). DLK also suppresses neuronal degeneration as DLK activation following a conditioning lesion in *Drosophila* larval PNS motoneurons protects axons from degeneration upon subsequent injuries (Xiong and Collins 2012). Homodimerisation of DLK is sufficient for its activation (Nihalani *et al.* 2000) and JIP1, another JIP family scaffold protein, maintains DLK in an inactive state in part by preventing its dimerization (Nihalani *et al.* 2003). Thus, the interaction of scaffolding molecules and kinases they scaffold can regulate the activity of the kinases involved in neuronal regeneration.

We investigated the role of a JIP family protein in regeneration. We show that UNC-16, the *Caenorhabditis elegans* JIP3 homolog (Byrd *et al.* 2001), inhibits regeneration of touch neurons after axotomy. The faster regeneration in *unc-16* mutants is a result of quicker initiation of neuronal regrowth and is independent of Kinesin-1, Dynein, and JNK-1 but is dependent on DLK-1. Our data suggest that UNC-16 independently and in a concentration-dependent manner, inhibits regeneration by acting on the regeneration-promoting long isoform of DLK-1. UNC-16's inhibitory effect on the long DLK-1 isoform is independent of and in addition to the inhibition by the short DLK-1 isoform. UNC-16 negatively regulates actin dynamics dependent on DLK-1 and microtubule dynamics partially dependent on DLK-1. Microtubule and actin dynamics in *unc-16* mutants, post-injury, are also partially dependent on CEBP-1, a transcription factor with key roles in DLK-1 dependent neuronal regeneration (Yan *et al.* 2009; Li *et al.* 2015).

We also show that the faster regeneration seen upon loss of UNC-16 does not translate into functional recovery, but slower regeneration observed when UNC-16 is over-expressed shows functional recovery compared to wild-type animals. The dual inhibitory control by both UNC-16 and the short isoform of DLK-1 may balance the intrinsic growth-promoting function of the long isoform of DLK-1 *in vivo* and a slower regeneration rate through modulation of cytoskeletal dynamics may assist in functional recovery of the injured neuron.

Materials and methods

Strains

Caenorhabditis elegans strains were grown on NGM agar plates seeded with *Escherichia coli* OP50 bacteria at 16°C (Brenner 1974) (Table 1). *jkk-1p*::*T7*::*unc-16* plasmid was generated by inserting T7-UNC-16 DNA excised from CMVT7p-UNC-16 plasmid (Byrd *et al.* 2001) into NHjkkp-1p, which was made by replacing *jkk-1p*::*gfp* DNA region of MK104p (Kawasaki *et al.* 1999) with multiple cloning sites. *ofm-1p*::DsRed-monomer has been described previously (Arimoto *et al.* 2011). The homozygosity of all MosSCI* (single-copy insertion of a transgene into a defined site) strains was confirmed using PCR before and after completion of the axotomy assays using reported primers (Yan and Jin 2012).

Laser axotomy

Nanosecond laser (Spitlight 600, Innolas, Munich, Germany) pulses ($\lambda = 355$ nm) of energy 0.8 μJ in single-shot mode was used to generate neuronal cuts (Rao *et al.* 2008). One of the posterior lateral mechanosensory (PLM) neurons expressing soluble GFP was cut approximately 30–50 μm away from the cell body. All experiments were done using larval stage 4 animals grown at 16°C. We chose this temperature as the *unc16(tb109)* mutants show accelerated growth and we wanted to ensure that we capture the characteristics of neuronal regeneration in *unc-16(tb109)* mutants vis-à-vis wild type. Our experiments were carried out 9 h post-axotomy as they gave us clear differences between genotypes, data are represented as percentage regeneration that refers to the number of animals that show neuronal regeneration.

Imaging and analysis

Images for analysis were acquired using a 100X objective, 1.4 NA at 1 × 1 binning, and were processed using ImageJ software. Regeneration was represented as percent neuronal regeneration *i.e.*, number of neuronal processes showing regrowth out of total number of axotomized neurons (Hammarlund *et al.* 2009; Nix *et al.* 2011). The length of the regrowing process was measured from the cut site (Wu *et al.* 2007; Zou *et al.* 2013). Neurons showing >4 μm regrowth were considered as regenerating. Imaging was done 9 h post-axotomy unless otherwise mentioned.

Statistical analysis

The data have been represented as mean ± s.e.m. The data when represented as % regeneration is an average of at least two separate trials. One-way ANOVA was used as a test of significance unless specified otherwise. P-values < 0.05 were considered as significant.

Localization of GFP tagged DLK isoforms

PLM neurons of one-day adult animals were imaged using a Perkin Elmer spinning-disc confocal microscope (488 nm laser, objective 100X, 1.4 NA) with an EMCCD C9100-13 camera.

Microtubule and actin dynamics measurement

Laser axotomy was performed using a ns-pulsed Nd-YAG LASER at 355 nm and energy 0.8 mJ (Litron Nano S60-30) using a 60X, 1.35 NA objective. The axotomy was performed on *juIs338* or *wyIs291* L4 animals 100 μm from the cell body. The animals were washed with M9 buffer and rescued. At the reported time point, the animals were anesthetized with 5 mM Levamisole and imaged using 488 nm laser excitation with a Yokogawa CSU-X1-A3 spinning disc confocal head and a Hamamatsu C9100-13 EMCCD Camera controlled by Volocity collectively supplied by PerkinElmer. Imaging was done under 100X 1.4 NA objective using 300 ms exposure at 3 frames/s for a total of 3 min for *juIs338* and 600 ms exposure at 1.6 frames/s for a total of 3 min for *wyIs291*. Kymographs were generated using the ImageJ plugin MultiKymograph (Schindelin *et al.*, 2012). We measure the total number of EBP-2::GFP comets which are visualized as sloped lines in kymographs. The sloped lines were also used to calculate the length and direction of the comets. We measured three parameters, viz., the density of immobile actin-rich regions, number of actin trails and actin trail length as described earlier (Sakamoto *et al.* 2005; Ganguly *et al.* 2015). EBP-2::GFP comets and GFP::utCH trails with polymerizing length above 0.3 μm were used for total number, speed, and length of EBP-2::GFP comet. The total number of EBP-2::GFP comets and GFP::utCH trails were then normalized to the duration of the image file as well as the length of the ROI in focus to generate the normalized microtubule dynamics graph. Immobile actin-rich regions are visible in distance and time kymograph plots as vertical lines and actin trails as sloped lines.

Table 1 List of *C. elegans* strains

Strain	Genotype	Reference
SK4005	*zdIs5[mec-4p::GFP]*	Clark and Chiu (2003)
FF41	*unc-116(e2310)*	Patel *et al.* (1993)
CB109	*unc-16(e109)*	Brenner (1974)
TT130	*unc-16(tb109)* abbreviated as *unc-16(lf)*	Choudhary *et al.* (2017)
CZ3011	*unc-16(ju146)*	Byrd *et al.* (2001)
KG1758	*unc-16(ce451)*	Edwards *et al.* (2013)
MT1542	*unc-16(n730)*	Trent *et al.* (1983) and Byrd *et al.* (2001)
NM2417	*juIs162 (unc-16p::unc-16::gfp)*	Byrd *et al.* (2001)
VC8	*jnk-1(gk7)*	Villanueva *et al.* (2001)
CF702	*muIs32[mec-7p::gfp]*	Ch'ng *et al.* (2003)
CB57	*unc-14(e57)*	Brenner (1974)
NM1787	*dhc-1(js319)*	Koushika *et al.* (2004)
KU1000	*N2; kmEx1000 [jkk-1p::T7::UNC-16]*	Described above
CZ18975	*juIs338 [mec-4p::ebp-2::GFP]*	Ghosh-Roy *et al.* (2012)
CZ8920	*cebp-1(tm2807)* abbreviated as *cebp-1(0)* *wyIs291[unc-86p::GFP::utCH]*	Yan *et al.* (2009) Chia *et al.* (2014)
CZ11327	*dlk-1(ju476)zdIs5* abbreviated as *dlk-1(Only S)*	Yan and Jin (2012)
CZ16351	*dlk-1(tm4024)zdIs5* abbreviated as *dlk-1(0)*	
CZ11530	*juEx2529 [mec-4p::dlk-1(L)::gfp]*	
CZ15142*	*zdIs5; rgef-1p::dlk-1(L) (juSi50)* abbreviated as *Si(L)*	
CZ15144*	*dlk-1(ju476)zdIs5; rgef-1p::dlk-1(L) (juSi50)*	
CZ16440*	*dlk-1(tm4024)zdIs5; rgef-1p::dlk-1(L) (juSi50)*	
CZ15143*	*zdIs5; rgef-1p::dlk-1(S) (juSi46)* abbreviated as *Si(S)*	
CZ15145*	*dlk-1(ju476)zdIs5; rgef-1p::dlk-1(S) (juSi46)*	
CZ16352*	*dlk-1(tm4024)zdIs5; rgef-1p::dlk-1(S) (juSi46)*	

Behavioral assay

Laser axotomy was performed using a multiphoton IR laser (720 nm) on one PLM 50 µm away from the cell body. Two cuts were introduced 6 µm apart. A worm that is moving backward responds to a gentle touch to its posterior side by reversing its direction of locomotion (Chalfie *et al.* 1985). This touch assay was performed on both the sides (right and left) at 3, 9, and 24 h post axotomy where only one of the two PLM neurons was axotomized. The reversal response mediated by the side with the uninjured posterior touch neuron serves as an internal control for each animal whose behavior was assessed post-axotomy. Using this assay, one can measure touch sensation with a posterior touch response index (PTRI) (Basu *et al.* 2017) which has been plotted.

After ascertaining that there is no difference between PTRI of uncut and laser mock cut animals in all the genotypes tested, the touch assay was performed 3, 9, and 24 h post axotomy (Figure 9A). The PTRI was normalized to the unaxotomized PTRI of each genotype (Basu *et al.* 2017). The morphology assessment of the axotomized PLM was done after 24 h (Figure 9, B and C). For statistics, multiple column comparison of ANOVA, with Neumann Keul's *post-hoc* test was used. $^{*}P < 0.01$, $^{**}P < 0.001$, and $^{***}P < 0.0001$.

Results

Loss of UNC-16 leads to an increase in neuronal regeneration

To study UNC-16's role in regeneration, we compared the post-axotomy regrowth in the posterior lateral microtubule (PLM) neuron of *unc-16* mutants and wild-type animals. All six alleles viz., *ce451*, *ju146*, *e109*, *tb109*, *n730*, and *km75* of *unc-16*, showed greater number of animals whose neurons regenerate as compared to wild type (Figure 1A) (Byrd *et al.* 2001; Edwards *et al.* 2013; Choudhary *et al.* 2017). This is similar to the inhibitory effect reported for *unc-16* mutants in *C. elegans* motor neuron regeneration (Chen *et al.* 2011; Nix *et al.* 2014). *tb109*, *n730*, and *km75* have stop codons which are predicted to truncate the protein at different lengths (Figure 1A). All six alleles also showed reduced *unc-16* RNA levels compared to wild type (Supplementary Figure S1). The inhibitory effect of *unc-16* on neuronal regeneration is not allele specific varying from 43% to 88% in different loss of function (lf) alleles. The alleles *tb109* and *ju146* had strong phenotypes and hence were chosen for further analysis.

We found that expression of a transgene that encodes UNC-16::GFP (Byrd *et al.* 2001) or T7::UNC-16 (*jkk-1p::T7::unc-16*) in *unc-16(tb109)* mutants reduces regeneration from 81% to 27% (Figure 1A). Furthermore, expression of UNC-16::GFP or T7::UNC-16 in wild-type animals resulted in 19% of the severed processes regenerating compared to 36% in wild type. This suggests that the presence and levels of UNC-16 is sufficient to inhibit regeneration following injury.

Loss of UNC-16 results in faster initiation of regeneration

To examine the time course of regeneration in *unc-16* mutants, we monitored the neuronal processes of *unc-16(tb109)* and *unc-16(ju146)* mutants at different time points after axotomy. At 6 h, 38% of *unc-16(ju146)* and 57% of *unc-16(tb109)* mutants initiated neuronal regrowth compared to only 16% in wild type (Figure 1, B and C). Furthermore, neuronal outgrowth in both alleles of *unc-16* mutants examined, started earlier at 3 h post axotomy, unlike in wild-type injured axons, where it began at 6 h (Figure 1, B and D). At 9 h, *unc-16(ju146)* and *unc-16(tb109)* mutants showed a ~2.6 and ~6.7 fold significantly greater neuronal process length compared to wild type (Figure 1B). The increase in the number of animals showing regrowth and the greater length of neuronal outgrowth, together, show that loss of *unc-16* promotes earlier initiation of regrowth. Over-expression of UNC-16 in neurons did not alter the time when regrowth was initiated, where growth began similar to wild-type animals at 6 h post-axotomy (Figure 1D).

We also examined the rate of regrowth after initiation by measuring the length of the regrowing axon at defined times after axotomy. Six to nine hours post-axotomy, the neuronal processes in *unc-16(tb109)* mutants grew at the rate of 2.1 µm/h,

significantly higher than the wild-type neuronal growth rate of 0.6 μm/h (Figure 1E). The difference in growth rate between wild-type (1.7 μm/h) and *unc-16(tb109)* (6.4 μm/h) mutants was greatest in the 9–12-h time interval post-axotomy. We also evaluated the growth rate in *unc-16(ju146)* mutants and found similar trends (Figure 1E). Elevating UNC-16 levels using a transgene expressing T7:: UNC-16 reduces the growth rate (Figure 1E), eventually resulting in shorter process lengths 24 h post-axotomy (Figure 1D).

At 18 h post-axotomy, the neuronal regrowth rate in *unc-16(tb109)* mutants was reduced and became comparable to wild type (Figure 1E). Twenty-four hours post-axotomy, more than 50% of the processes of *unc-16(tb109)* mutants show several branches (Figure 1C), some that overlap with the distal process; thus, an accurate assessment of true growth rates is not measurable. Taken together our data suggest that the loss of *unc-16* results in a quicker initiation of regrowth and a faster rate of process regrowth up to 12 h post-axotomy. These data suggest that UNC-16 acts as an inhibitory factor in the early steps of axon regeneration and prevents regrowth initiation and slows the rate of axon extension after injury.

Increased regeneration in *unc-16* depends on DLK-1

UNC-16 is a scaffolding protein that plays multiple roles in intracellular transport and MAPK signaling. It interacts with the Kinesin-1 motor (Sun *et al.* 2011), the Dynein motor (Arimoto *et al.* 2011), an RUN domain protein UNC-14 (Sakamoto *et al.* 2005), a leucine-rich repeat kinase 2 (LRRK2) (Hsu *et al.* 2010; Choudhary *et al.* 2017) and MAP kinases such as JNK-1 (Kelkar *et al.* 2000) and DLK (Ghosh *et al.* 2011). We thus examined if regeneration in UNC-16 depends on the above proteins.

We assessed neuronal regeneration in loss-of-function (lf) mutants of the Kinesin heavy chain-1 (*unc-116*), the JNK MAP kinase (*jnk-1*), RUN domain protein (*unc-14*), leucine-rich repeat kinase 2 (*lrk-1*), Dynein heavy chain (*dhc-1*), and the Dual-leucine zipper kinase (*dlk-1*). The single mutants either regenerate similarly to wild type, as seen in the *unc-116* and the *jnk-1* mutants or regenerate significantly less than wild type as seen in mutants of *unc-14*, *lrk-1*, *dhc-1*, and *dlk-1* (Figure 2A, Supplementary Figures S2 and S3). In addition, double mutants between *unc-16(tb109)* and the above-mentioned genes did not alter UNC-16-dependent regeneration (Figure 2A, Supplementary Figures S2 and S3) except in *unc-16; dlk-1* double mutants. We examined the effect of loss of UNC-16 in different alleles of *dlk-1* (Figure 2A, Supplementary Figure S4). The milder *dlk-1* alleles *ju477* and *ju591* (Yan and Jin 2012) (Supplementary Figure S4) do not affect regeneration on their own, but they inhibit regeneration in *unc-16(tb109)* mutants. Regeneration in *dlk-1; unc-16(lf)* double mutants built with stronger alleles of *dlk-1*, viz. *ju476* and *tm4024*, is completely abolished (Figure 2A). Thus, the inhibitory role of UNC-16 in neuronal regeneration is dependent on DLK-1.

UNC-16 inhibits the regeneration-promoting function of DLK-1L

DLK is an essential MAPKKK that initiates regrowth of neuronal processes after injury and in growth cone formation in many model systems (Hammarlund *et al.* 2009; Yan *et al.* 2009; Xiong *et al.* 2010; Wang and Jin 2011; Shin *et al.* 2012). *dlk-1* in *C. elegans* encodes two isoforms, DLK-1L (long) and DLK-1S (short), that have antagonistic functions. DLK-1S forms a heterodimer with DLK-1L and inactivates the regeneration-promoting role of DLK-1L (Yan and Jin 2012) (Supplementary Figure S4). JIPs are known to scaffold and regulate MAP kinases and in particular, the family member, JIP3, the mammalian orthologue of UNC-16, is known to form a complex with DLK (Kelkar *et al.* 2000; Holland *et al.* 2016). Hence, we investigated whether UNC-16 influences neuronal regeneration through a specific isoform of DLK-1.

Neuronal regeneration is dependent on DLK-1 levels (Hammarlund *et al.* 2009; Yan *et al.* 2009) and our observations could be influenced by variable expression, typical of extrachromosomal transgenic lines. Hence we used animals with single-copy integrated transgenic expression of DLK-1S or DLK-1L made using the Mos-SCI technique (Yan and Jin 2012) to assess the effect of DLK-1S or DLK-1L in *unc-16* mutants. Comparable to previous studies, single copy transgenic expression of DLK-1S or DLK-1L in wild-type animals, respectively suppresses or enhances neuronal regeneration even at 9 h post-axotomy (Figure 2B) (Yan and Jin 2012). The allele *dlk-1(ju476)* does not express DLK-1L but expresses endogenous levels of intact DLK-1S and is referred to as *dlk-1(onlyS)* and the allele *dlk-1(tm4024)* (a DLK-1 null) is referred to as *dlk-1(0)*. These alleles are an useful tool to determine whether regeneration in *unc-16* mutants is influenced by DLK-1S or DLK-1L.

To determine if DLK-1S and UNC-16 act independently to inhibit DLK-1L mediated regeneration, we assessed regeneration in the following genotypes: single copy DLK-1L with *dlk-1(onlyS); unc-16(lf)* and *dlk-1(0); unc-16(lf)*. Single copy DLK-1L is introduced so that some regeneration occurs allowing us to assess the inhibitory effects of DLK-1S and UNC-16. *unc-16(lf)* mutants lacking DLK-1S show significantly higher regeneration compared to animals that contain DLK-1S, suggesting that DLK-1S and UNC-16 can both inhibit DLK-1L (Figure 2B).

To examine whether UNC-16 can act independently of DLK-1S, regeneration was assessed in animals expressing DLK-1L in *dlk-1(0)* or *dlk-1(0); unc-16(lf)*. We observed greater regeneration in *dlk-1(0); unc-16(lf)* compared with *dlk-1(0)* and the difference was greatest at 6 h post-axotomy consistent with UNC-16's early role in regeneration (Figure 2B). We observed that loss of *unc-16* is unable to promote regeneration in animals expressing DLK-1S in wild type, *dlk-1(onlyS)* or *dlk-1(0)* mutant backgrounds (Figure 2B). However, animals expressing DLK-1L in *dlk-1(onlyS); unc-16(lf)* double mutants exhibited increased regeneration compared with animals expressing DLK-1L in *dlk-1(onlyS)* mutants alone (Figure 2B). In the presence of single copy of DLK-1S, the loss of UNC-16 leads to a twofold increase in regeneration in *dlk-1(onlyS)* mutants and a further 1.5-fold increase in regeneration in *dlk-1(0)* mutants (Figure 2B). This suggests that DLK-1S and UNC-16 act independently, to inhibit regeneration. However, in *dlk-1(0)* mutants, 6 h post-axotomy, these differences were not significant (Figure 2C), and this may be due to the larger amounts of DLK-1L available in the single copy DLK-1L line, soon after axotomy, resulting in faster initiation of regeneration.

Our data show that UNC-16 inhibits the growth-promoting activity of DLK-1L. We have shown that UNC-16 acts independently and in addition to DLK-1S to inhibit regeneration (Figure 2, B and C) and the inhibition by overexpression of DLK-1S is not suppressed by the *unc-16(lf)* mutation (Figure 2C).

UNC-16 changes the localization of DLK-1L

Vertebrate DLK, *C. elegans* GFP::DLK-1L, GFP::DLK-1S and endogenous UNC-16 are all shown to localize in punctae along the neuron (Yan and Jin 2012; Edwards *et al.* 2013; Holland *et al.* 2016). The punctate localization of vertebrate DLK has been shown to depend on palmitoylation-dependent binding of DLK to JIP3 (Holland *et al.* 2016). Therefore, we examined the localization of

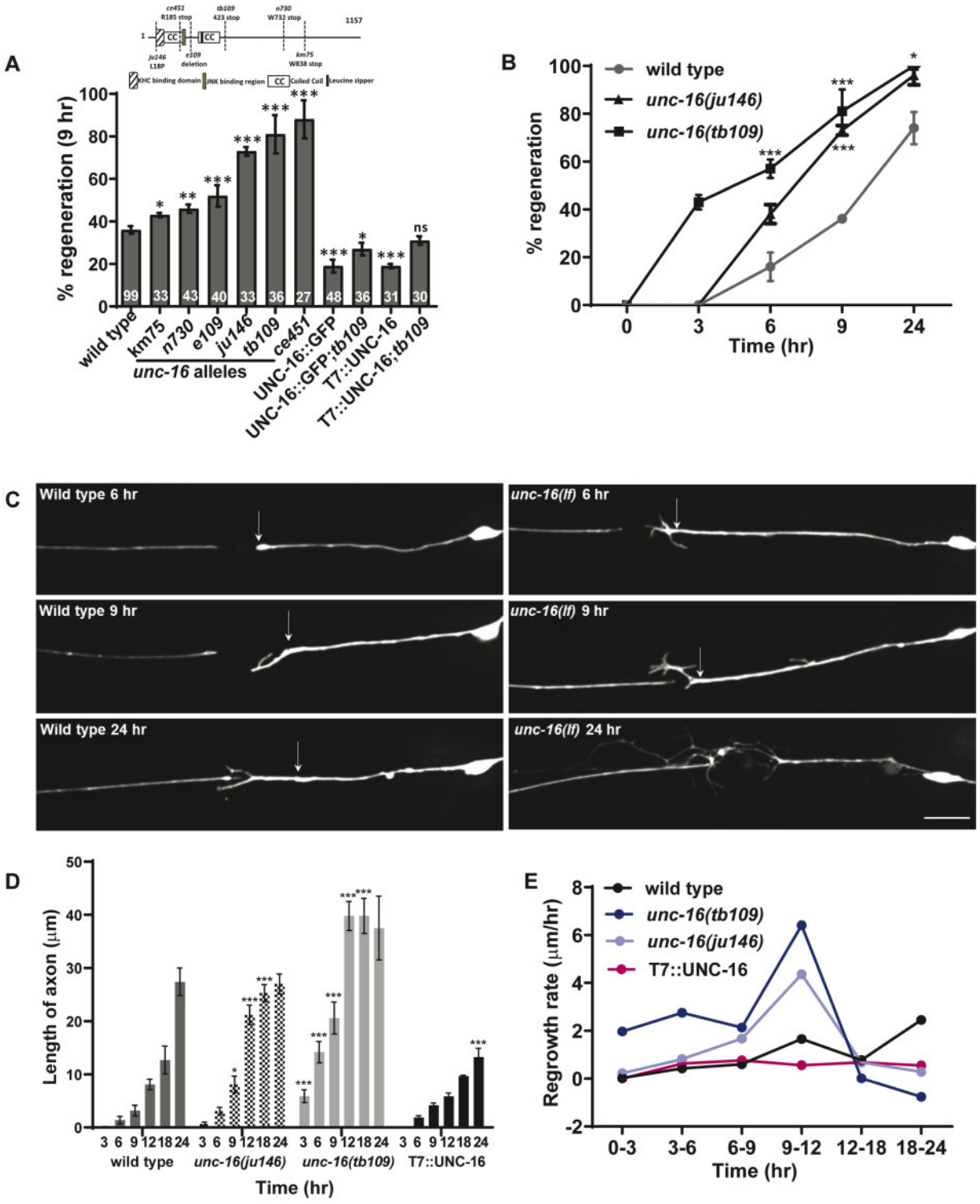

Figure 1 Loss of UNC-16/JIP3 promotes neuronal regeneration. (A) Percentage of neurons regenerating post-axotomy in *unc-16* alleles and in wild type and *unc-16(tb109)* mutants upon expression of UNC-16::GFP (expressed under the *unc-16* promoter) and T7::UNC-16 (expressed under the *jkk-1* promoter). Inset: UNC-16 domain structure and location of mutations in *unc-16* mutant alleles. (B) Percentage of neurons regenerating at different time points post-axotomy in wild type, *unc-16(ju146)* mutants and *unc-16(tb109)* mutants. (C) Representative images of the PLM touch neuron process at different time points post-axotomy in wild type and *unc-16(tb109)* mutants. Arrow indicates axotomy location. Scale bar 10 μm. (D) Length of the regenerated neuronal process at different time points after axotomy. (E) Regrowth rate of the neuronal process in each 3-h interval after axotomy. One-way ANOVA, *P*-value *<0.05, **<0.005, ***<0.001. Number of animals inside bars in (A). Number of animals is 20 for (B, D, and E).

DLK-1L in both *unc-16(tb109)* and in neurons with increased levels of UNC-16.

The punctate localization of GFP::DLK-1L is reduced in all six *unc-16* alleles examined with stops before and after the MAPK binding domain (Figure 3, A and B, Supplementary Figures S1A and S5). Further, upon UNC-16 over-expression, GFP::DLK-1L showed a significant increase in the intensity of puncta in wild type and in *dlk-1(0)* mutants. This indicates an increase in

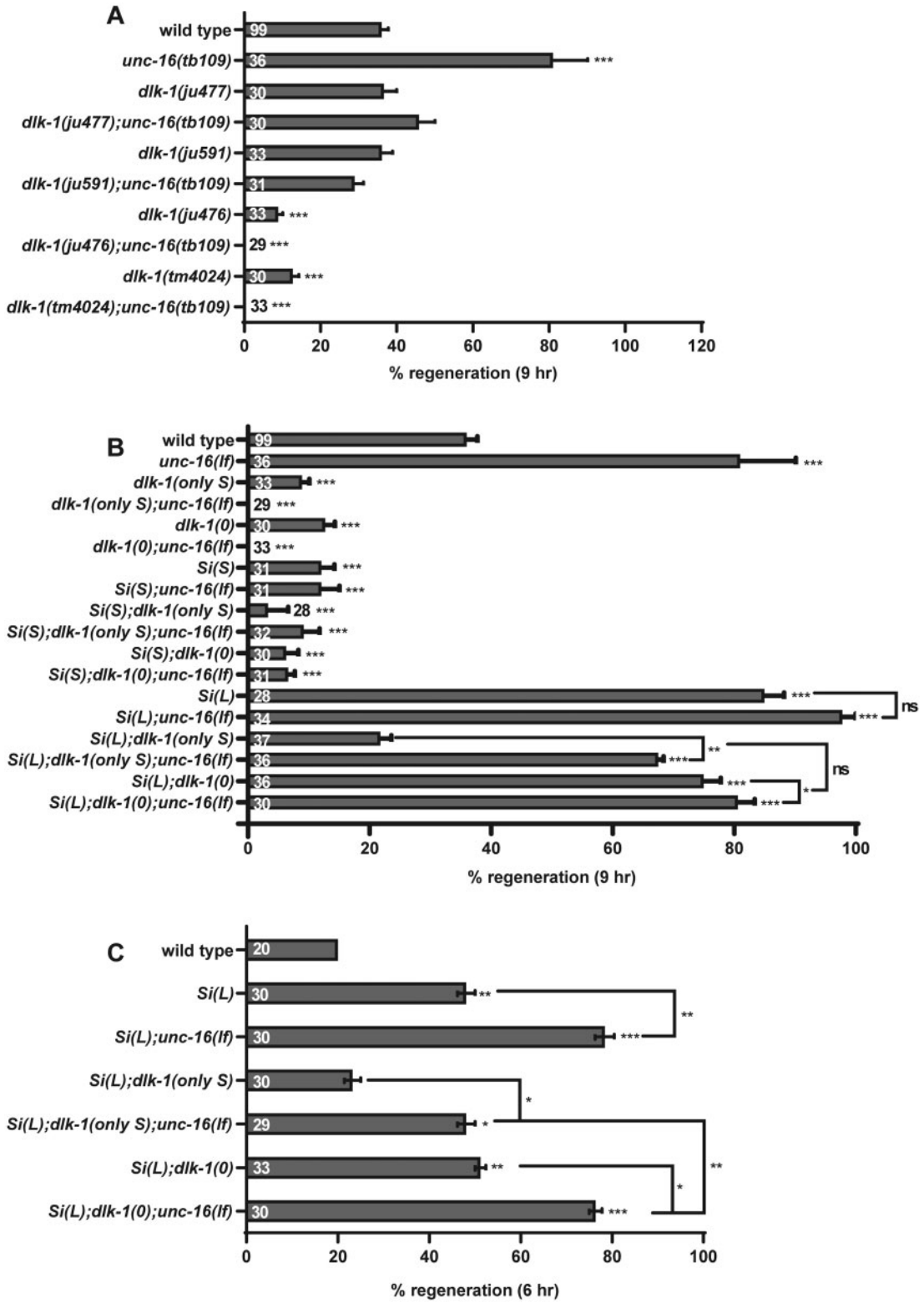

Figure 2 UNC-16 inhibits DLK-1L. (A) Effect of *unc-16(tb109)* mutation on regeneration phenotype of various alleles of *dlk-1*. (B) Genetic analysis of regeneration in *unc-16(tb109)*, the null *dlk-1(tm4024)* [*dlk-1(0)*] and *dlk-1(ju476)* [*dlk-1(Only S)*] mutants, expressing single copy transgene of *MosSci* DLK-1L [*Si(L)*] or *MosSci* DLK-1S [*Si(S)*] 9 h post-axotomy. ns: not significant. (C) Genetic analysis of effect of *unc-16(tb109)* mutation on animals expressing a single copy *MosSci* DLK-1L in wild type and *dlk-1(tm4024)* mutant background 6 h post-axotomy. One-way ANOVA, *P*-value *<0.05, **<0.005, ***<0.001. Number of animals inside bars.

GFP::DLK-1L in each puncta in the presence of excess UNC-16, however, the density of the puncta remains unaffected at ~2.5 ± 0.4/10 µm remaining similar to wild type (Figure 3, A and B). Our observations show that the punctate DLK-1L localization is dependent on the presence and levels of UNC-16 (Figure 3, A and B). We see that mutations in multiple places in UNC-16, both

preceding and following the MAPK binding domain (Figure 1A, inset), lead to changes in localization of DLK-1.

The punctate localization of *C. elegans* GFP::DLK-1S has been shown to depend on its association with DLK-1L (Yan and Jin 2012). GFP::DLK-1S, similar to GFP::DLK-1L, is not punctate in *unc-16(lf)* mutants (Supplementary Figures S6 and S7). Surprisingly, DLK-1S is punctate upon over-expression of T7::UNC-16 in the absence of DLK-1L, *i.e.*, in a *dlk-1(null)* background (Supplementary Figures S6 and S7). This indicates that UNC-16 facilitates the punctate localization of DLK-1L and DLK-1S independent of each other, although our experiments cannot address whether DLK-1L and 1S are present together in these punctae.

Upon axotomy, DLK-1L is known to increase locally at the injury site while DLK-1S does not (Yan and Jin 2012). We examined whether the post-axotomy localization of DLK-1L is dependent on UNC-16 and whether the localization of DLK-1L along the axon is altered post axotomy. Comparable to the previous mentioned study, we observe that 4 min after axotomy, the levels of GFP::DLK-1L at the proximal end of the cut site increase (Figure 3, C and D). However, in *unc-16(lf)* mutants there is a greater accumulation of GFP::DLK-1L at the proximal cut site (Figure 3, C and D) compared to wild type at the same time point. Furthermore, overexpression of UNC-16 leads to a significant reduction of GFP::DLK-1L accumulation at the proximal cut site with the GFP::DLK-1L signal comparable to the GFP alone control (Figure 3, C and D). Thus, the presence and levels of UNC-16 controls the post-axotomy levels of DLK-1L at the cut site. In addition, the intensity of DLK-1L punctae along the neuronal process ~10 μm away from the injury site is reduced (Figure 3C). The extent of reduction in intensity depends on the presence and levels of UNC-16 (Figure 3C).

The UNC-16-dependent localization of DLK-1L before injury and UNC-16-dependent control of DLK-1L levels post-injury at the cut site and along the neuronal process suggests that UNC-16 may inhibit DLK-1L function along the axon. The release of DLK-1L from the punctae may be stimulated by injury signals such as Ca^{+2} known to regulate DLK-1L (Yan and Jin 2012).

Microtubule dynamics after injury in *unc-16* mutants are partially dependent on DLK-1

DLK-1 is known to enable neuronal regeneration through two independent pathways, by elevating microtubule dynamics and by regulating transcription through CEBP-1 (Yan *et al.* 2009; Ghosh-Roy *et al.* 2010; Nix *et al.* 2011; Li *et al.* 2015; Tang and Chisholm 2016) (Figure 9D). We assessed microtubule dynamics using EBP-2::GFP, a marker for the growing plus end of microtubules (Ghosh-Roy *et al.* 2012).

In wild-type animals, the number of EBP-2::GFP comets pre-immediately and post-axotomy in a 40 μm region adjacent to the axotomy site are similar (Figure 4, A and C, Supplementary Videos S1 and S2). 3 and 6 h post-axotomy the number of EBP-2::GFP comets show a 2- and 2.5-fold significant increase (Figure 4, A and C) comparable to earlier reports (Ghosh-Roy *et al.* 2012). In wild-type animals, the length of the EBP-2::GFP comet tracks shows a peak increase at 2 h post-axotomy that remains elevated until 6 h post-injury (Figure 4, B and C). In *dlk-1(0)* mutant neurons, the number of EBP-2::GFP comets are fewer than in wild-type animals pre-axotomy, and do not significantly increase even 6 h post-axotomy (Figure 4C, Supplementary Table S1). We observe a similar trend where EBP-2::GFP track length increases 3 h post-axotomy but at 6 h post-axotomy, there is no change compared to the uninjured neurons of *dlk-1(0)* mutants.

We assessed the effect of *unc-16(lf)* on microtubule dynamics pre- and post-axotomy. We observe that there is an elevation in the number of EBP-2::GFP comets in uninjured neurons of *unc-16(lf)* mutant (Figure 4C, Supplementary Table S1) suggesting that UNC-16 downregulates microtubule dynamics. In uninjured neurons of the double mutant *dlk-1(0); unc-16(lf)* the number of EBP-2::GFP comets continues to have an 1.5-fold significant increase similar to that seen in the *unc-16(lf)* mutant, suggesting that the change in microtubule dynamics in *unc-16* uninjured neurons is independent of DLK-1.

After injury the number of EBP-2::GFP comets show nearly a twofold increase 6 h in *unc-16(lf)* close to the 2.5-fold increase seen in wild-type axotomized processes at a similar time point (Figure 4C). The length of the EBP-2::GFP comet trails is increased in wild type, *dlk-1(0)*, *unc-16(lf)* and *dlk-1(0); unc-16(lf)* mutants, 3 h post-axotomy (Supplementary Figure S8). In all the genotypes tested, there is no significant difference in the direction of microtubule growth compared to wild type (Supplementary Figure S9). Although regeneration in *unc-16(lf)* mutants is completely dependent on DLK-1 (Figure 2A), microtubule dynamics in *unc-16(lf)* mutants are only partially dependent on DLK-1 after axotomy. Since regeneration in *unc-16(lf)* mutants is fully DLK-1 dependent, it suggests that factors other than microtubules could contribute to DLK-1 dependent regeneration in *unc-16(lf)* mutants.

Actin dynamics and growth cone protrusions post-injury in *unc-16* mutants are dependent on DLK-1

Actin, the actin depolymerizing factor (ADF)/cofilin A and non-muscle Myosin II that powers actin's retrograde flow, are all important for growth cone formation and for the extension of both developing and regenerating vertebrate neurons (Hur *et al.* 2011; Flynn *et al.* 2012; Chisholm *et al.* 2016; Blanquie and Bradke 2018; Tedeschi *et al.* 2019). Thus, we followed actin dynamics by using a transgenic line that expresses the GFP tagged calponin homology domain of F-actin-binding protein Utrophin (GFP::utCH) (Burkel *et al.* 2007; Chia *et al.* 2014; Sood *et al.* 2018).

The number of GFP::utCH trails in wild-type neurons increases significantly, 3 h post-axotomy, in both anterograde and retrograde directions (Figure 5B). In the 40 μm region proximal to the injury site, the length of all GFP::utCH trails also increases 2 h post-axotomy (Figure 5A, Supplementary Videos S3 and S4). In wild-type neurons, the density of actin-rich regions reduces significantly 3 h post-axotomy (Figure 5C). Unlike microtubule dynamics that show regional changes (Ghosh-Roy *et al.* 2012), actin dynamics change throughout the proximal injured neuron 3 h post-axotomy. We observe an increase in the length of all GFP::utCH trails (Figure 6A) and a decrease in actin-rich regions throughout the proximal injured axon (Figure 6B). The density of actin-rich regions reduces the most in the proximal 30–60 μm next to the axotomy site 3 h post-axotomy (Figure 6B). The number of GFP::utCH trails increases the most 60–90 μm away from the site of axotomy (Figure 6C).

The number and length of anterograde and retrograde actin trails in uninjured neurons of wild type and *dlk-1(0)* mutants is comparable (Figure 7, B and C). The density of actin-rich regions in uninjured *dlk-1(0)* mutant neurons is similar to that seen in wild type (Figure 7A). Three hours post-axotomy, there is no statistically significant change in density of actin-rich regions, numbers, or lengths of actin trails in *dlk-1(0)* mutant neurons compared to *dlk-1(0)* uninjured neurons (Figure 7, Supplementary Table S2). This shows that changes in actin dynamics post-injury are dependent on DLK-1.

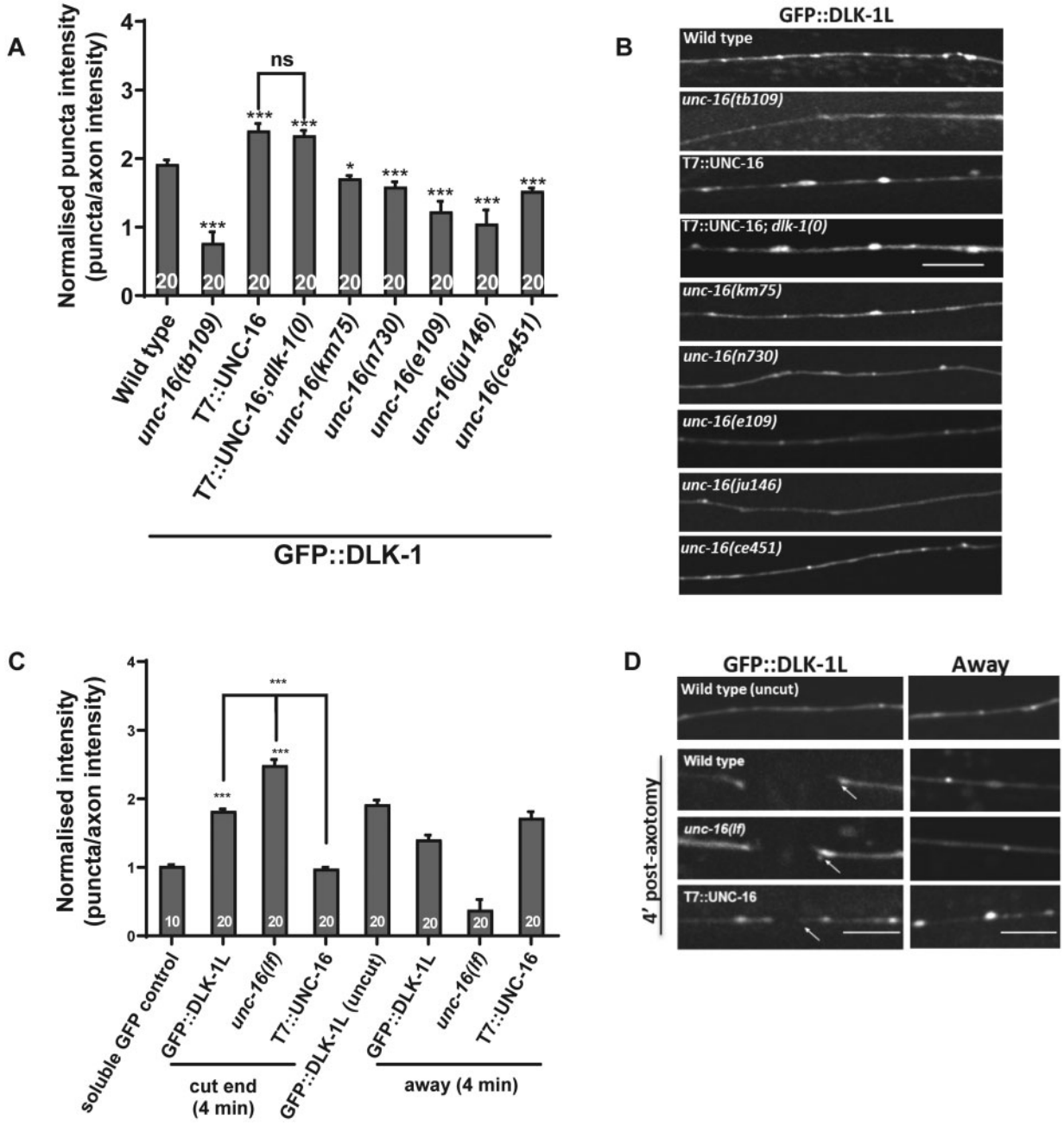

Figure 3 UNC-16 regulates DLK-1L localization in a dose-dependent manner. (A) Normalised intensity of DLK-1::GFP in different *unc-16(tb109)* mutants and animals expressing T7::UNC-16 (expressed under the *jkk-1* promoter) in wild type and the null *dlk-1(tm4024)* mutants. Intensity of mCherry expressed form *mec-4p::mCherry* was used as a negative soluble marker control. (B) Representative images of GFP::DLK-1L localization quantified in (A) Scale bar 10 μm. (C) Normalized intensity of GFP::DLK-1L in the first 3 μm near the proximal cut end of an axotomized PLM touch neuron and ~10 μm away from the injury site in wild type, T7::UNC-16 (expressed from *jkk-1p::T7::unc-16*) and *unc-16(tb109)* mutants. (D) Representative images of axotomized PLM touch neurons expressing GFP::DLK-1L, 4 min post-axotomy at and away from the site of axotomy. Arrow points to the proximal cut end with respect to cell body. Scale bar 5 μm. One-way ANOVA, *P*-value *<0.05, ***<0.001. Number of animals inside bars.

We then assessed the GFP::utCH dynamics in *unc-16(lf)* mutant touch receptor neurons. The number of GFP::utCH trails in uncut *unc-16(lf)* mutants is similar to that seen in wild-type animals (Figure 7B). However, the length of the GFP::utCH trails increased fivefold in uninjured *unc-16(lf)* mutant neurons compared to wild type (Figure 7C). The density of GFP::utCH marked actin-rich regions is reduced by ~50% in uninjured *unc-16(lf)* mutant neurons compared to wild type, perhaps contributing to the polymerizing F-actin pools in the neuronal process seen in this genotype (Figure 7A).

In *unc-16(lf)* mutant neurons 3 h after axotomy, the numbers of trails are ~1.3-fold greater compared to wild type and nearly twofold higher than actin trails seen in uninjured *unc-16(lf)* mutant neurons (Figure 7B). Three hours post-injury, the length of the GFP::utCH trails in *unc-16(lf)* mutant neurons is similar to that seen in wild-type neurons at the same time point (Figure 7C). In all the genotypes tested, the increase in GFP::utCH trails occurs in both anterograde and retrograde directions. Interestingly 3 h post-axotomy, *unc-16(lf)* mutant neurons showed no significant reduction in density of actin-rich regions compared to uninjured

unc-16(lf) neurons (Figure 7A). By contrast, in wild-type neurons there is a significant reduction in density of actin-rich regions post-axotomy.

Neurons in *dlk-1(0); unc-16(lf)* double mutants were indistinguishable from the *dlk-1(0)* mutant neurons and show no increase in number, length, or density of GFP::utCH trails in both uninjured neurons or 3 h post axotomy (Figure 7) suggesting that the actin dynamics in *unc-16(lf)* mutant neurons are dependent on DLK-1 both before and after injury.

We also investigated whether the altered actin dynamics changes the structure of the neuronal growth cone. Hence, we counted the number of filipodial protrusions in growing post-axotomized neurons from wild type, *unc-16(lf)*, *dlk-1(0)*, and *dlk-1(0); unc-16(lf)* mutant animals. We observe that in *unc-16(lf)*

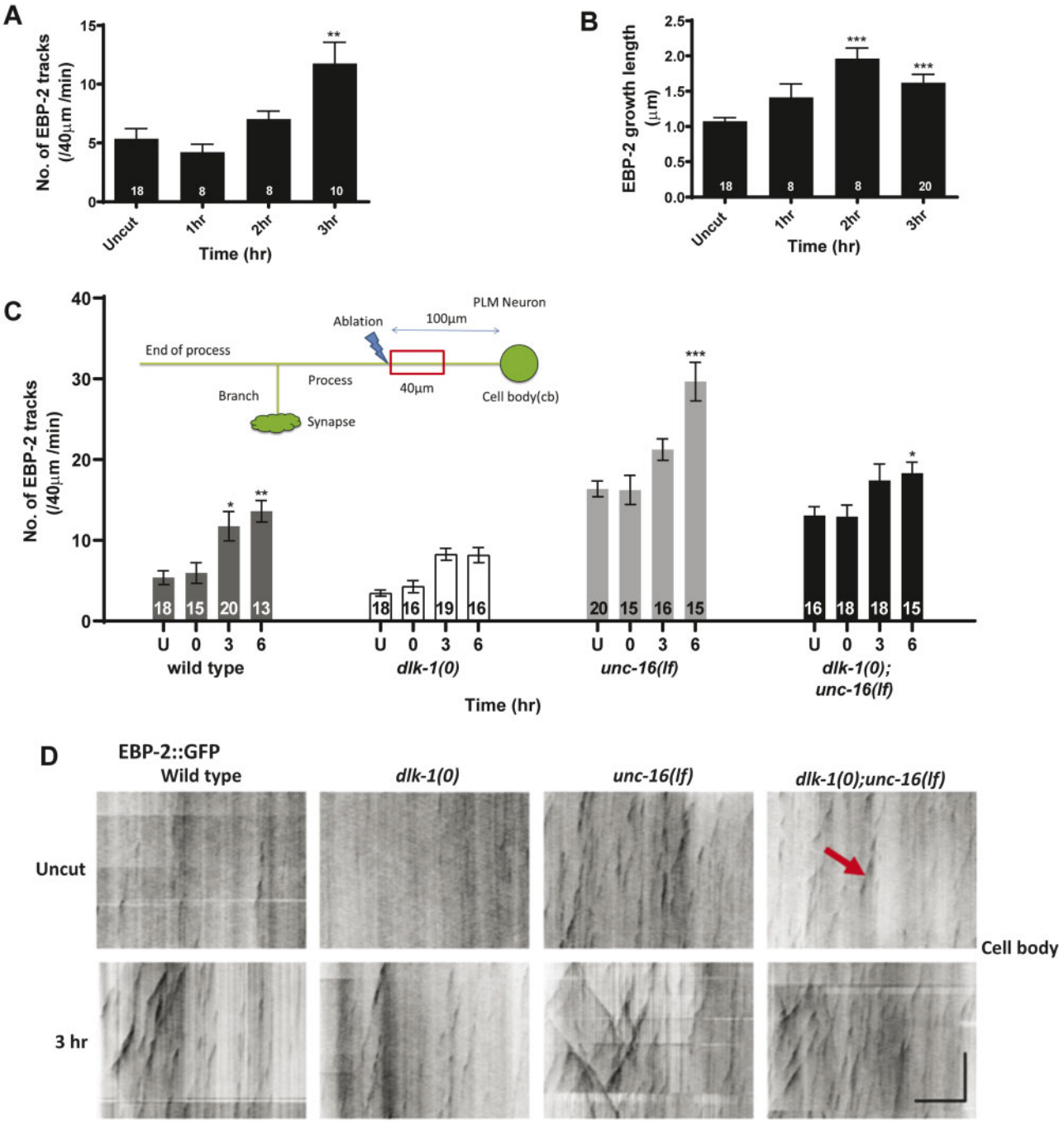

Figure 4 UNC-16 inhibits microtubule dynamics. (A) Number of EBP-2::GFP tracks in uncut and axotomized wild-type animals as a function of time, up to 3 h post injury. (B) Change in length of EBP-2::GFP tracks in uncut and axotomized wild-type animals across a 3 h post-injury period. Number of animals inside bars. One-way ANOVA with Bonferroni correction, *P*-value *<0.05, **<0.01, ***<0.001. (C) Numbers of EBP-2::GFP tracks in kymographs before and after axotomy in wild type, *unc-16(tb109)*, *dlk-1(tm4024)* and double mutant *dlk-1(tm4024); unc-16(tb109)* in uncut and different time points post-axotomy. Two-way ANOVA with Bonferroni correction, *P*-value *<0.05, **<0.01, ***<0.001. Inset: Schematic of the touch neuron indicating the area of ablation and region of imaging. (D) EBP-2::GFP kymographs from uncut and 3 h post-injury neurons in wild type, *dlk-1(tm4024)*, *unc-16(tb109)*, and double mutant *dlk-1(tm4024); unc-16(tb109)*. The length (*x*-axis) and time (*y*-axis) scales are 10 µm and 25 s, respectively. Red arrow indicates an EBP-2 trail.

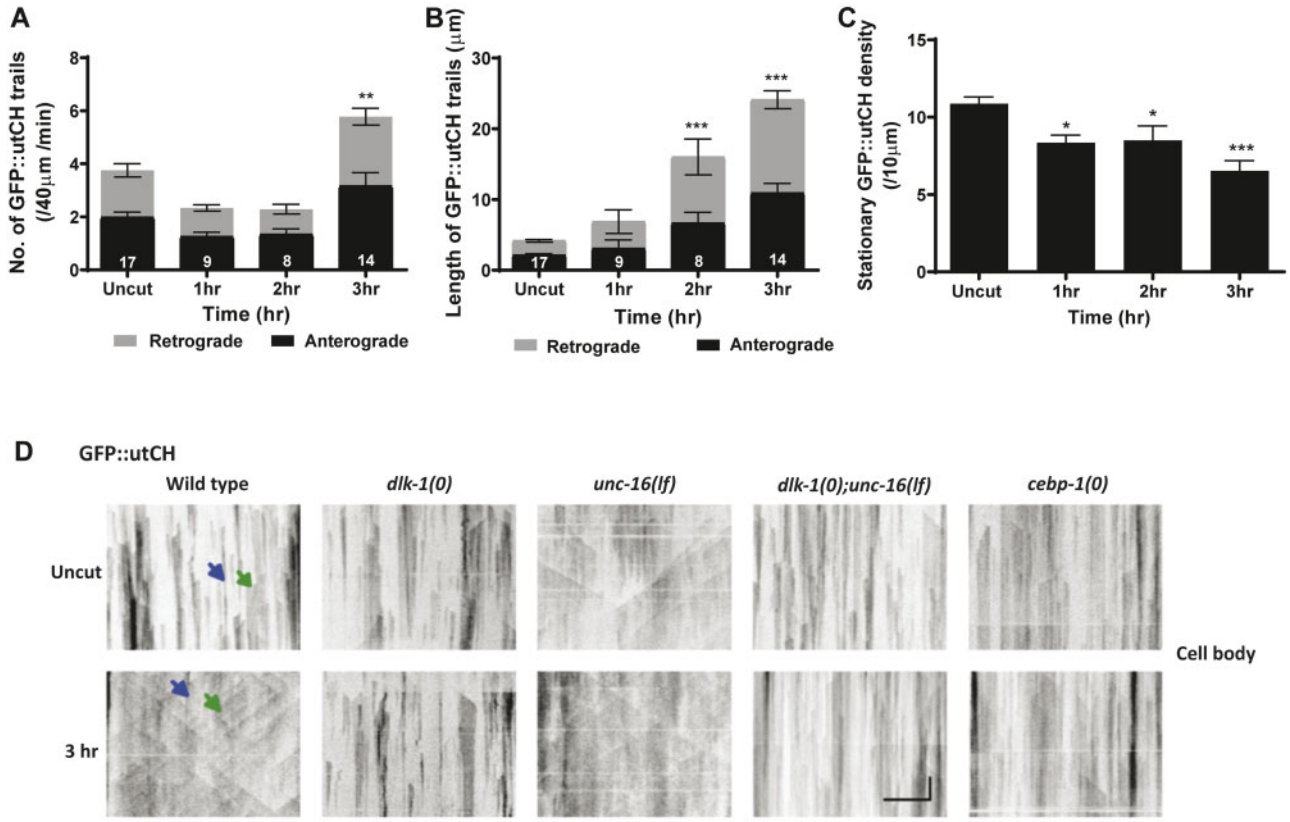

Figure 5 Temporal changes in actin dynamics in the injured neuronal process. (A) Number of GFP::utCH trails in wild type uncut neurons and 40 μm adjacent to the injury site of wild-type neurons up to 3 h post-injury. (B) Change in length of GFP::utCH trails in anterograde and retrograde directions in neurons and 40 μm adjacent to the injury site of wild-type neurons up to 3 h post-injury. (C) Comparison of the density of stationary GFP::utCH stationary clusters in neurons of uncut and axotomized wild-type animals over time period of 3 h post injury. Number of animals inside bars. One-way ANOVA with Bonferroni correction, *P*-value **<0.01, ***<0.001. (D) Representative kymographs of GFP::utCH in wild type, *dlk-1(tm4024)*, *unc-16(tb109)*, the double mutant *dlk-1(tm4024); unc-16(tb109)* and *cebp-1 (tm2807)* mutants, uninjured and 3 h post injury in PLM touch neuron. Blue arrows indicate stationary utCH clusters and green arrows indicate a utCH trail. The length (*x*-axis) and time (*y*-axis) scales are 10 μm and 25 s, respectively.

mutants, the genotype with greatest increase in actin dynamics pre- and post-axotomy, also shows an increase in the number of filipodial protrusions after injury compared to all remaining genotypes examined (Supplementary Figures S10 and S11). This elevation in filipodial protrusions in *unc-16(lf)* mutants begins 6 h post-axotomy (Supplementary Figure S12). Wild-type neurons show greater number of protrusions at the growth cone compared to neurons from *dlk-1(0)* mutants (Supplementary Figure S11). In *dlk-1(0); unc-16(lf)* double mutants, the number of filipodial protrusions are similar to the number seen in *dlk-1(0)* mutant neurons (Supplementary Figure S11). Thus, increased actin dynamics pre- and post-axotomy may alter the growth cone morphology. Actin dynamics likely make significant contributions to the increased regeneration in *unc-16* mutants, lack of regeneration in *dlk-1* mutants and the lack of regeneration in *dlk-1; unc-16* double mutants.

Post-axotomy actin and microtubule dynamics in *unc-16* mutants partially depend on CEBP-1

DLK-1 is known to affect neuronal regeneration by promoting translation and stabilization of CEBP-1 mRNA in touch neurons (Yan *et al.* 2009) (Figure 9D). CEBP-1 along with another transcription factor ETS-4 activates other growth factors necessary for neuronal outgrowth during regeneration (Li *et al.* 2015). Thus, we examined if the microtubule and actin dynamics seen in *unc-16* mutants also depend on CEBP-1.

We measured EBP-2 dynamics in wild type, *unc-16(lf)*, *cebp-1(0)* and *unc-16(lf); cebp-1(0)* mutants. Uninjured neurons in *unc-16(lf)* mutants have an increased number of EBP-2 comets (Figure 8B) compared to wild-type animals while *cebp-1(0)* and *unc-16(lf); cebp-1(0)* mutants are similar to wild type. This suggests that microtubule dynamics in uninjured UNC-16 neurons are dependent on CEBP-1.

Post-axotomy, the *cebp-1(0)* mutant neurons do not show any significant change in the number of EBP-2 comets (Ghosh-Roy *et al.* 2012) (Figure 8B). After injury, *unc-16(lf); cebp-1(0)* mutant neurons show a significant decrease in the number of EBP-2 comets, compared to *unc-16(lf)* mutants (Figure 8B). All genotypes show an increase in EBP-2 comet growth length 6 h post-axotomy (Figure 8A). Thus, in *unc-16(lf)* mutants, basal microtubule dynamics are fully dependent on CEBP-1 but the elevation in microtubule dynamics post-injury is only partially dependent on CEBP-1.

We also examined whether actin dynamics post-injury are dependent on CEBP-1. Actin dynamics in *cebp-1(0)* mutant neurons are indistinguishable from *dlk-1(0)* mutant neurons pre- or post-axotomy (Figure 7). Post-axotomy the number of GFP::utCH trails in neurons from *unc-16(lf); cebp-1(0)* mutants is significantly lower than that seen in *unc-16(lf)* mutants and significantly higher than that seen in *cebp-1(0)* mutants (Figure 7B, Supplementary Table S3). The length of the GFP::utCH trails in the *cebp-1(0)* mutants post-axotomy is greatly reduced compared to wild type and stays

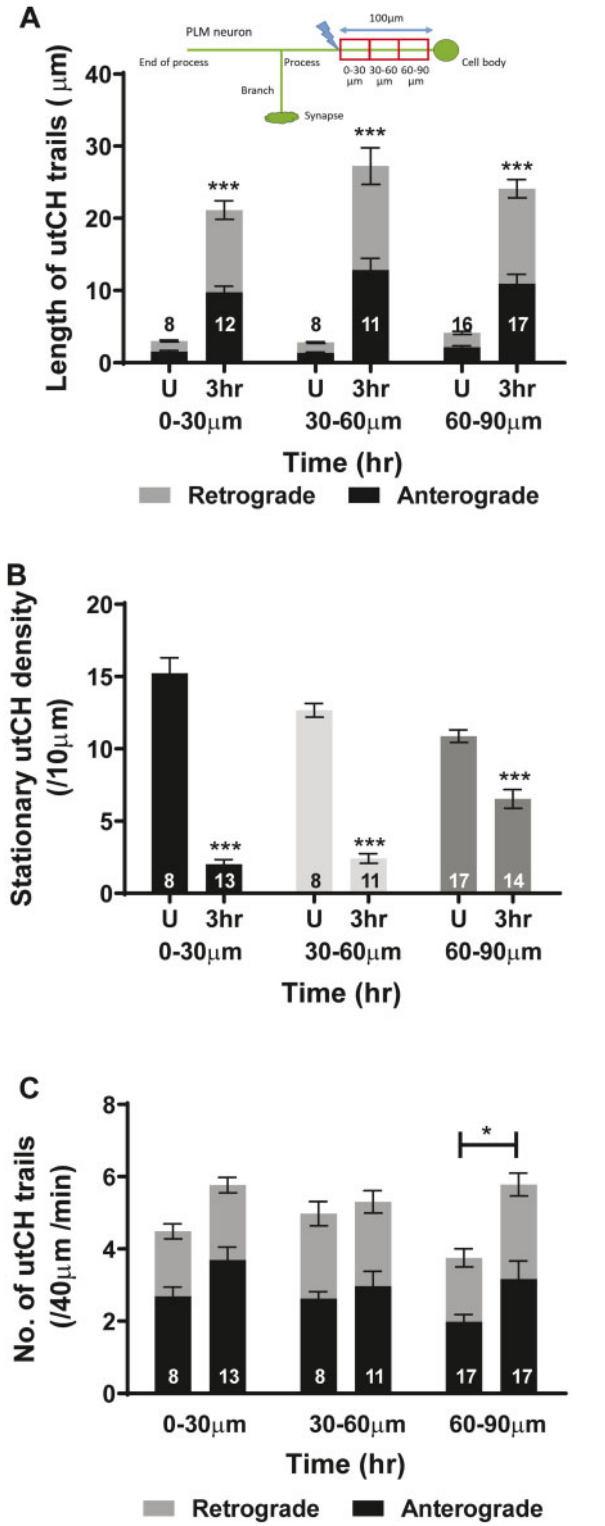

Figure 6 Actin dynamics are altered in the entire proximal axotomized neuronal process. (A) Change in length of GFP::utCH trails in uncut and axotomized wild-type animals at 3 h post injury over the entire section of the neuron in anterograde and retrograde direction. Inset: Schematic of the touch neuron indicating the area of ablation and regions of imaging. (B) Comparison of the density of stationary GFP::utCH in uncut and axotomized wild-type animals 3 h post injury in various sections of the neuron. (C) Number of GFP::utCH trails in uncut and axotomized wild type 3 h post injury over various sections of the neuron in anterograde and retrograde direction. Number of animals inside bars. Two-way ANOVA with Bonferroni correction (A, B, D, and F), one-way ANOVA with Bonferroni correction (C, E), *P*-value *<0.05, ***<0.001.

unchanged in the *unc-16(lf); cebp-1(0)* double mutants (Figure 7C). We conclude that regulation of actin dynamics in *unc-16* mutants occurs partially through CEBP-1, suggesting that actin regulation can occur independently of changes in microtubule dynamics, potentially through CEBP-1's action on regulators of actin.

cebp-1(0) mutants show reduced regeneration compared to wild type (Figure 8C). We observed that despite complete absence of CEBP-1, the *unc-16(lf); cebp-1(0)* double mutants show a twofold higher regeneration compared to *cebp-1(0)* mutants, 9 hr post-axotomy (*P*-value 0.04) (Figure 8C). The partial regeneration seen in *unc-16(lf); cebp-1(0)* double mutants likely arise from the continued small increase in microtubule and actin dynamics seen in these animals.

Functional recovery of the regenerating neuron

Functional regeneration post-axotomy has been observed in *C. elegans* motor and touch neurons (Ben-Yakar *et al.* 2009; Abay *et al.* 2017; Basu *et al.* 2017; Ding and Hammarlund 2018). More specifically, the axonal fusion of the proximal and distal ends of touch neurons post-injury has been shown to be responsible for the observed functional regeneration in touch neurons (Abay *et al.* 2017; Basu *et al.* 2017). Since loss of UNC-16 causes faster regrowth, we examined whether it led to quicker functional regeneration.

The bilaterally symmetric PLM neurons mediate a gentle touch escape response and is represented as PTRI (Basu *et al.* 2017). In the wild-type worms, 3 h post-axotomy, there is a significant decrease of the touch response on the axotomized side compared to the response on the side of animals with uncut PLM neuron (Figure 9A). This lowered PTRI recovered significantly 24 h post injury and about 38% of the injured wild-type PLM neurons show fusion between the proximal and distal processes (Figure 9, B and C).

In *unc-16(lf)* mutants, upon axotomy, there is a significant decrease in touch response on the axotomized neuron side compared to the touch responsiveness on the uninjured side leading to a lower PTRI (Figure 9A). However, there is no significant increase in PTRI from 3 to 24 h after injury, thus there is an absence of significant functional recovery after injury despite greater neuronal outgrowth (Figure 9A). Concurrently, we observe that only 14.5% of the injured neurons show fusion between the distal and proximal ends (Figure 9B). In animals expressing T7::UNC-16 we found a significant decrease in PTRI 3 h after injury compared to the uncut worms of the same genotype (Figure 9A). After 24 h there is a significant increase in PTRI from 3 h and we observe about 26.3% fusion at this time point (Figure 9B). Although the number of neurons that show fusion is slightly lower in T7::UNC-16, it is not statistically significant compared to wild type (*P*-value of 0.13), and the PTRI at 24 h is comparable to wild type.

Taken together these data show that although there is faster growth in *unc-16(lf)* mutants, it does not translate into increased functional regeneration. In contrast, in animals overexpressing UNC-16, though the growth rate is significantly reduced, slower regrowth is observed to support significant functional recovery 24 h post-axotomy. Thus, rapid rates of regeneration in an injured axon may not necessarily lead to better functional recovery. Furthermore, excessive sprouting in *unc-16(lf)* mutants (Supplementary Figures S10 and S11) may reduce fusion events important for functional recovery.

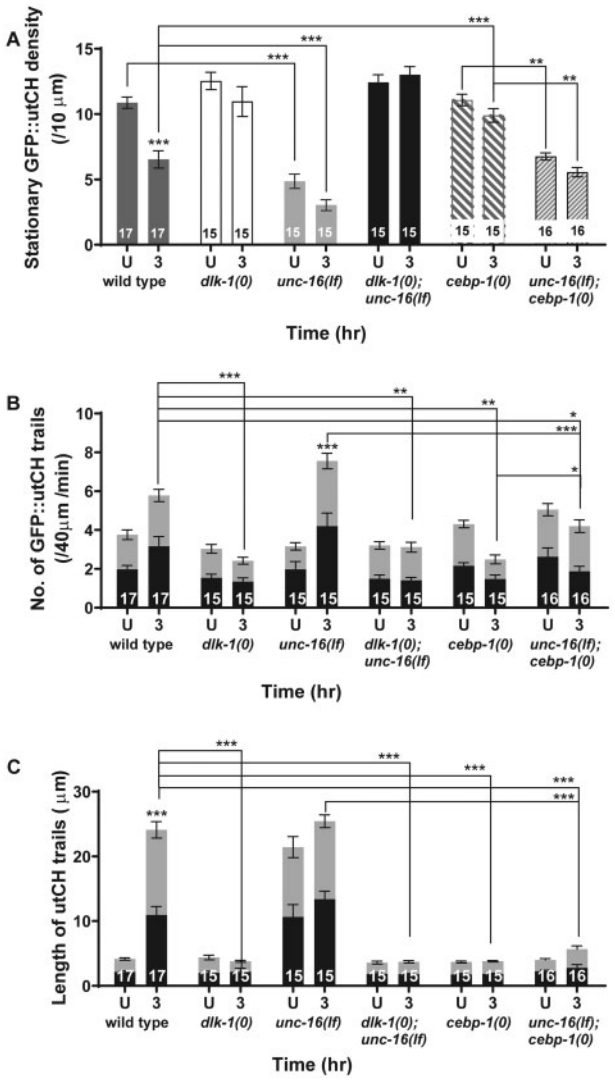

Figure 7 Actin dynamics in *unc-16* mutants are dependent on DLK-1 and CEBP-1. (A) Comparison of the density of stationary GFP::utCH in uncut and 3 h post injury neurons in wild type, *unc-16(tb109)*, *dlk-1(tm4024)* and *cebp-1(tm2807)* and double mutants *dlk-1(tm4024); unc-16(tb109)* and *cebp-1(tm2807); unc-16(tb109)*. (B) Number of GFP::utCH trails in uncut and 3 h post injury neurons in various genotypes in the anterograde and retrograde directions. (C) Comparison of the length of GFP::utCH trails in uncut and 3 h post injury neurons in various genotypes in the anterograde and retrograde direction. Number of animals inside bars. One-way ANOVA with Bonferroni correction (A), two-way ANOVA with Bonferroni correction (B, C), *P*-value *<0.05, **<0.01, ***<0.001.

Discussion

Our study shows that UNC-16 plays an inhibitory role on regeneration where its presence and levels act early to control both growth initiation and regrowth rate. These effects are dependent on the MAPKKK DLK-1, essential for regeneration in multiple models (Hammarlund *et al.* 2009; Itoh *et al.* 2009; Yan *et al.* 2009; Xiong *et al.* 2010; Nix *et al.* 2011; Shin *et al.* 2012). There are few known inhibitors that act directly on DLK, the master regulator of regeneration (Hammarlund *et al.* 2009; Valakh *et al.* 2015; Chisholm *et al.* 2016; Asghari Adib *et al.*, 2018). Our study suggests that UNC-16/JIP3 acts by making DLK-1 unavailable along the neuronal process to control the levels of DLK-1 at the injury site. This study identifies the role of DLK-1-dependent actin dynamics as an important mediator of axonal regeneration. In addition, UNC-16 dependent microtubule dynamics are regulated partially by CEBP-1 in both uninjured and injured neurons. Our data suggest that UNC-16 acts like a clamp on cytoskeletal dynamics, negatively regulating both microtubule and actin dynamics. Intriguingly, the rapid regrowth, at least partially mediated by altered cytoskeletal dynamics, does not promote functional recovery. Our study identifies a key role for UNC-16 in balancing the rate of axon regrowth to enable functional recovery.

Systematic genetic screens in *C. elegans* identified that only ~10% of genes inhibit neuronal regeneration while 83% of genes identified in the screen promote neuronal growth post-injury (Chen *et al.* 2011). UNC-16/JIP3 is a negative regulator that acts on DLK-1L independently and in addition to the inhibitory isoform DLK-1S (Figure 3C) (Chen *et al.* 2011; Nix *et al.* 2014). Interestingly, JIP3 through its binding ability with Kinesin-1 has been shown to be necessary for axonal regeneration in sensory neurons (Watt *et al.* 2015). However, our data suggest that in the PLM touch neuron, Kinesin-1 by itself or in conjunction with UNC-16, does not appear to significantly influence axon regeneration (Supplementary Figure S2). UNC-16 was also identified as a negative regulator of regeneration in a screen for motor neuron regeneration in *C. elegans* (Chen *et al.* 2011; Nix *et al.* 2014). JIP3, by the virtue of being a scaffold protein is capable of binding to multiple regulators in the process of regeneration and thereby could play pivotal roles in regulating neuronal regeneration (Watt *et al.* 2015; Zeke *et al.* 2016).

Although vertebrate JIP3 is also known to form a complex with DLK (Kelkar *et al.* 2000; Holland *et al.* 2016), the effects of UNC-16 on DLK-1L in *C. elegans* may not be direct since several *unc-16* alleles independent of their predicted MAPKKK binding ability still influence both DLK-1 localization and regeneration (Figures 1A and 3, A and B). Apart from JIP3, DLK-1S is the only known inhibitor of DLK-1L (Yan and Jin 2012). Although the inhibitory DLK-1S like isoform has been suggested to be present in humans, its presence has not been verified in other organisms (Supplementary Table S4). Other identified negative regulators of regeneration like DIP-2 and NMAT-2 act through other parallel pathways and not directly on DLK-1 (Kim *et al.* 2018; Noblett *et al.* 2019). Thus, UNC-16 and its vertebrate homolog JIP3 may act as a general inhibitor of DLK mediated signaling in multiple species by altering its localization in an injury-dependent manner. UNC-16 may merely control DLK-1 availability at the injury site rather than regulate its kinase activity.

Cytoskeletal damage is thought to trigger DLK activity that subsequently initiates regeneration post injury (Valakh *et al.* 2015). Despite differences in pathways downstream of DLK-1 in regulating both microtubule and actin dynamics, regrowth after injury is likely to depend on the interaction between the actin and microtubule cytoskeletons during growth cone formation (Dogterom and Koenderink 2019). Our data suggest that the initiation of regrowth may require both microtubule and actin dynamics and both dynamics change at similar time scales after injury (Figures 4–7). DLK-1 is known to regulate local microtubule dynamics close to the injury site through the depolymerizing kinesin-13 family member, KLP-7 (Ghosh-Roy *et al.* 2012). Thus, some of the increased microtubule dynamics observed in *unc-16* mutants may be dependent on KLP-7. In addition, *unc-16* mutants also show increased microtubule dynamics partially dependent on DLK-1 (Figures 4C and 7A). However, the dependence of increased microtubule dynamics in *unc-16* mutants on KLP-7 remains to be investigated.

Cytoskeletal dynamics are increased in *unc-16(lf)* mutants. The increased microtubule dynamics persist post-axotomy but are

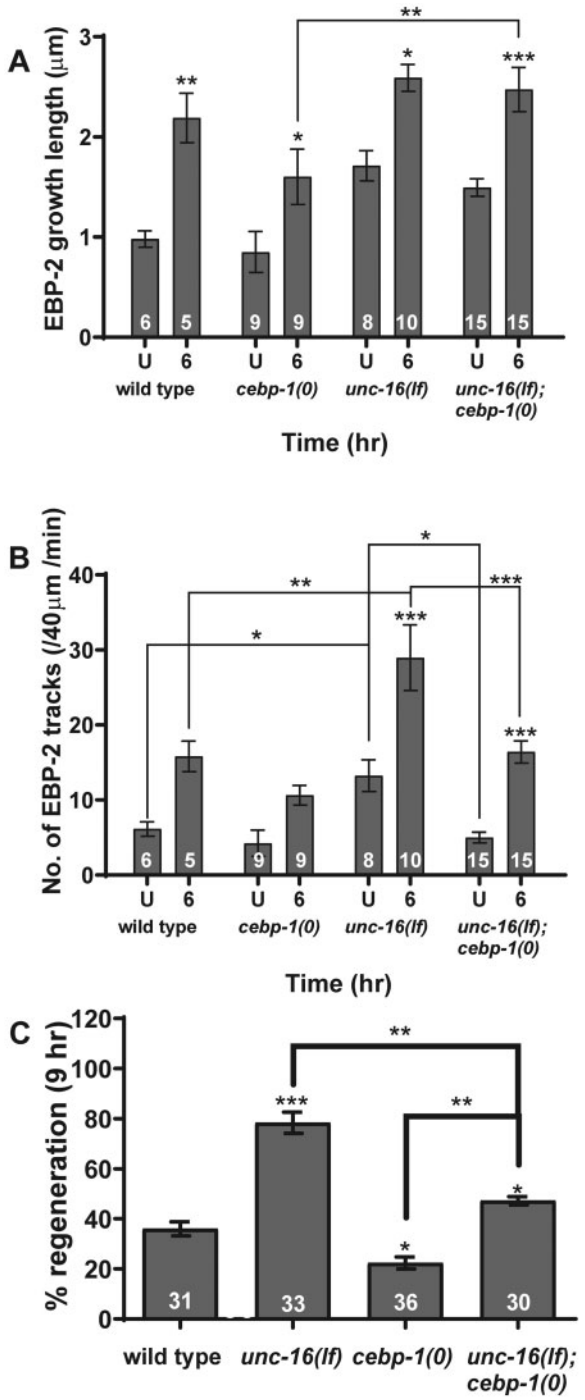

Figure 8 CEBP-1 regulates post-injury microtubule dynamics and regeneration. (A) Change in length of EBP-2::GFP tracks in uncut and axotomized wild-type animals, *unc-16(tb109)*, *dlk-1(tm4024)* and *cebp-1(tm2807)* and *cebp-1(tm2807); unc-16(tb109)* 6 h post injury. Number of animals inside bars. (B) Numbers of EBP-2::GFP tracks in kymographs before and after axotomy in wild type and other mutants in uncut and 6 h post injury. One-way ANOVA with Bonferroni correction, *P*-value *<0.05, **<0.01, ***<0.001. (C) Neuronal regeneration in wild type, *unc-16(tb109)*, *cebp-1(tm2807)*, and *cebp-1(tm2807); unc-16(tb109)*. One-way ANOVA *P*-value *<0.05, **<0.005, ***<0.001. Number of animals inside bars.

largely independent of DLK-1. By contrast, actin dynamics in *unc-16(lf)* mutants are also increased but are fully dependent on DLK-1. Because regeneration in *unc-16(lf)* mutants is dependent on DLK-1 (Figure 2A), regulation of actin dynamics via DLK-1 may be critical for the greater regeneration seen in *unc-16(lf)* mutants. However, the increased microtubule dynamics in *unc-16* mutants may also play a DLK-1-independent role in regeneration, for instance in controlling the rate of axon outgrowth.

Actin is thought to be important in the regenerating growth cone (Hur *et al.* 2011; Flynn *et al.* 2012; Chisholm *et al.* 2016; Blanquie and Bradke 2018; Tedeschi *et al.* 2019). Overexpression of the ADF/cofilin has been shown to induce regeneration in culture as well as *in vivo* following spinal cord injury (Tedeschi *et al.* 2019). Inhibition of nonmuscle myosin II, which powers retrograde actin flow in the growth cone, markedly enhances axon growth by reorganizing the growth cone cytoskeleton in cultured vertebrate neurons (Hur *et al.* 2011). The altered actin dynamics seen in *unc-16* mutants may occur through molecules such as Cofilin, Myosin II and actin polymerizers such as Formin and ARP2/3 (Hur *et al.* 2011; Flynn *et al.* 2012; Breitsprecher and Goode 2013; Chisholm *et al.* 2016; Blanquie and Bradke 2018; Tedeschi *et al.* 2019).

Our data suggest that UNC-16 controls actin dynamics partially through CEBP-1 (Figure 7). The transcription factor C/EBP, in other models, is known to be dependent on MAP kinases other than DLK-1 (Yamamoto *et al.* 1999). In *unc-16(lf); cebp-1(0)* double mutants microtubule dynamics are reduced. This suggests that there is a pathway by which CEBP-1 regulates basal microtubule dynamics. Actin dynamics are abrogated in *cebp-1(0)* mutants and remains so in *unc-16(lf); cebp-1(0)* double mutants (Figure 7). There is also a modest increase in number of actin trails compared to *cebp-1(0)* mutants (Figure 7B). Therefore, regeneration is higher than that seen in *cebp-1(0)* mutants but lower than observed in *unc-16(lf)* mutants. Thus, CEBP-1 has effects on both actin dynamics and on basal levels of microtubule dynamics in *unc-16(lf)* mutants.

Based on our findings we think that there are DLK-1 independent and dependent pathways for microtubule dynamics (Figure 9D). The DLK-1-dependent pathway may act through CEBP-1. Actin dynamics are completely dependent on DLK-1 and partially dependent on CEBP-1, while microtubule dynamics are partially dependent on DLK-1 and CEBP-1. A basal level of microtubule dynamics is also controlled through CEBP-1. Cytoskeletal dynamics is controlled in a complex manner where basal cytoskeletal dynamics as well as post-injury cytoskeletal dynamics are controlled partially through DLK-1 and CEBP-1 but also independent of them. Our data suggest a complex regulation of actin and microtubule dynamics might be responsible for controlling rate of regeneration. It also highlights the importance of UNC-16 in the spatial and temporal control of DLK-1.

Based on prior studies and our findings, we propose a model where UNC-16/JIP3 plays its inhibitory role through tight temporal and spatial control of DLK-1 function (Figure 9D). The dual inhibitory control by both UNC-16 and DLK-1S balance the intrinsic growth-promoting function of DLK-1L *in vivo*. This intrinsic growth ability is likely achieved through a balance between the actin dynamics and microtubule stabilization at the growth cone that could also mediate rapid steering of the growth cone in a regenerating neuron (Hur *et al.* 2012; Blanquie and Bradke 2018). Our study reveals the role UNC-16 plays in the complex control of both, basal and post-injury cytoskeletal dynamics.

Axonal injury breaks the connection between the neuronal cell body and its post-synaptic targets disrupting its functions and potentially the behaviors that depend on the neuron (He and Jin 2016). In *C. elegans* there are multiple reports of partial

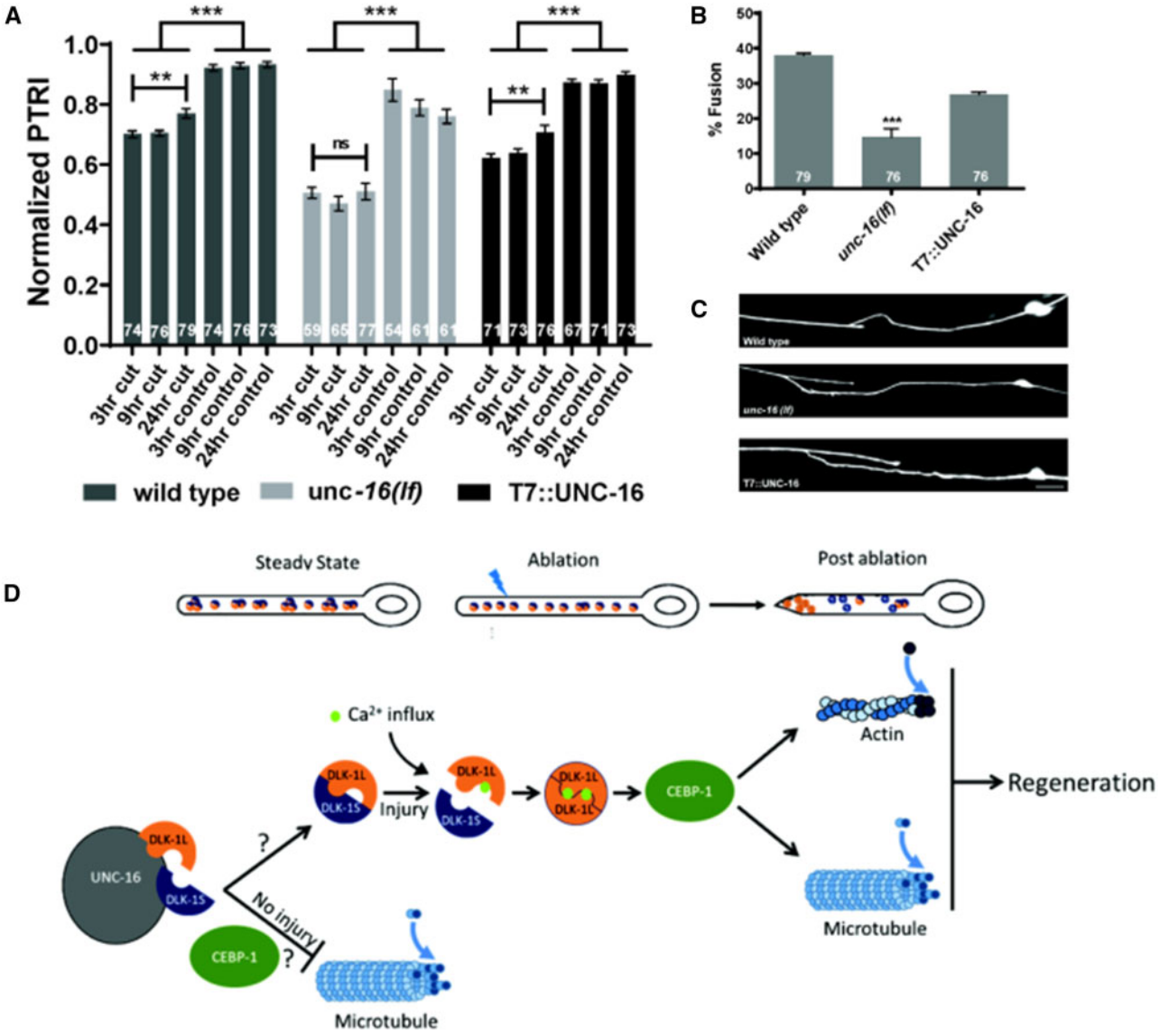

Figure 9 *unc-16(lf)* does not enhance functional recovery. (A) PTRI in axotomized and internal control neurons in wild type, *unc-16(tb109)* mutants and T7::UNC-16 (expressed by *jkk-1p::T7::unc-16*). Multiple column comparison of ANOVA, with Neumann Keul's *post-hoc* test *P*-value *<0.01, **<0.001, and ***<0.0001. ns: not significant. (B) Percentage of animals showing neuronal fusion of the proximal and distal end post-axotomy at 9 h in wild type, *unc-16(tb109)* mutants and T7::UNC-16 animals. One-way ANOVA *P*-value ***<0.001. Number of animals inside bars. (C) Representative images of neuronal fusion of the proximal and distal end post-axotomy at 9 h in wild type, *unc-16(tb109)* mutants and T7::UNC-16 animals. Scale bar 10 μm. (D) Suggested model of the mechanism of inhibition of neuronal regeneration by UNC-16.

recovery of locomotion following axotomy in multiple motor neurons (Yanik *et al.* 2004; Neumann *et al.* 2011; El Bejjani and Hammarlund 2012; Byrne *et al.* 2016).

We show that the faster regeneration seen in *unc-16(lf)* mutants does not lead to functional recovery known to depend on fusion of the distal and proximal parts of the injured neuron (Abay *et al.* 2017; Basu *et al.* 2017). The faster neuronal growth observed in *unc-16(lf)* mutants may not be favorable for fusion as it may adversely affect other required steps in restoring function, *e.g.*, cargo transport that is known to depend on UNC-16/JIP3 (Verhey *et al.* 2001; Sun *et al.* 2011). The *efa-6* mutant that shows faster regrowth and increased microtubule dynamics also does not show enhanced functional recovery (Chen *et al.* 2015; Basu *et al.* 2017). Furthermore, slower regeneration seen when UNC-16 is over-expressed shows functional recovery comparable to wild-type animals (Figures 1D and 9A). Thus, merely a faster rate of neuronal outgrowth is insufficient for functional recovery, highlighting the importance of mechanisms that modulate the growth rate of the regenerating neuron to allow for recovery of function.

Data availability

Strains and plasmids are available upon request. The authors affirm that all data necessary for confirming the conclusions of the article are present within the article, figures, and tables.

Supplementary material is available at *GENETICS* online.

Acknowledgments

The authors thank Y. Jin and K. Miller for strains. CGC provided strains and is funded by NIH Office of Research Infrastructure

Programs (P40 OD010440). They thank H. Krishnamurthy, M. Mathew at CIFF, NCBS. They also thank M. Kamak for illustrations, A. Ghose and G. Hasan for suggestions. S.S.K., V.S., S.S., and S.P.K. designed experiments, S.S.K., V.S., S.S., and A.B. performed experiments, K.M., N.H., and A.G-R. provided reagents and methodology, S.S.K. and S.P.K. wrote the manuscript. All authors read the manuscript.

Funding

Work supported by HHMI and DBT to S.P.K., CSIR to S.S.K. A.G.-R. lab is supported by the NBRC core fund from the Department of Biotechnology and Wellcome Trust-DBT India Alliance (Grant # IA/I/13/1/500874). The authors gratefully acknowledge support from Grant 12- R&D-IMS-5.02-0202 for the spinning disc confocal system to S.P.K., research costs supported by HHMI-IECS grant number 55007425, 1303/2/2019/R&D-II/DAE/2079, and BT/PR13938/BRB/10/795/2010 to S.P.K.

Conflicts of interest

The authors declare that there is no conflict of interests.

Literature cited

Abay ZC, Wong MY, Teoh JS, Vijayaraghavan T, Hilliard MA, *et al.* 2017. Phosphatidylserine save-me signals drive functional recovery of severed axons in *Caenorhabditis elegans*. Proc Natl Acad Sci USA. 114:E10196–E10205.

Arimoto M, Koushika SP, Choudhary BC, Li C, Matsumoto K, *et al.* 2011. The *Caenorhabditis elegans* JIP3 protein UNC-16 functions as an adaptor to link kinesin-1 with cytoplasmic dynein. J Neurosci. 31:2216–2224.

Asghari Adib E, Smithson LJ, Collins CA. 2018. An axonal stress response pathway: degenerative and regenerative signaling by DLK. Curr Opin Neurobiol. 53:110–119.

Basu A, Dey S, Puri D, Das Saha N, Sabharwal V, *et al.* 2017. let-7 miRNA controls CED-7 homotypic adhesion and EFF-1-mediated axonal self-fusion to restore touch sensation following injury. Proc Natl Acad Sci USA. 114:E10206–E10215.

Ben-Yakar A, Chronis N, Lu H. 2009. Microfluidics for the analysis of behavior, nerve regeneration, and neural cell biology in *C. elegans*. Curr Opin Neurobiol. 19:561–567.

Blanquie O, Bradke F. 2018. Cytoskeleton dynamics in axon regeneration. Curr Opin Neurobiol. 51:60–69.

Breitsprecher D, Goode BL. 2013. Formins at a glance. J Cell Sci. 126: 1–7.

Brenner S. 1974. The genetics of *Caenorhabditis elegans*. Genetics. 77: 71–94.

Burkel BM, von Dassow G, Bement WM. 2007. Versatile fluorescent probes for actin filaments based on the actin-binding domain of utrophin. Cell Motil Cytoskeleton. 64:822–832.

Byrd DT, Kawasaki M, Walcoff M, Hisamoto N, Matsumoto K, *et al.* 2001. UNC-16, a JNK-signaling scaffold protein, regulates vesicle transport in *C. elegans*. Neuron. 32:787–800.

Byrne AB, McWhirter RD, Sekine Y, Strittmatter SM, Miller DM, *et al.* 2016. Inhibiting poly(ADP-ribosylation) improves axon regeneration. Elife. 5:e12734.

Ch'ng QLim, Williams L, Lie YS, Sym M, Whangbo J, *et al.* 2003. Identification of genes that regulate a left-right asymmetric neuronal migration in *Caenorhabditis elegans*. Genetics. 164: 1355–1367.

Chalfie M, Sulston JE, White JG, Southgate E, Thomson JN, *et al.* 1985. The neural circuit for touch sensitivity in *Caenorhabditis elegans*. J Neurosci. 5:956–964.

Chen L, Chuang M, Koorman T, Boxem M, Jin Y, *et al.* 2015. Axon injury triggers EFA-6 mediated destabilization of axonal microtubules via TACC and doublecortin like kinase. Elife. 4:e08695.

Chen L, Wang Z, Ghosh-Roy A, Hubert T, Yan D, *et al.* 2011. Axon regeneration pathways identified by systematic genetic screening in *C. elegans*. Neuron. 71:1043–1057.

Chia PH, Chen B, Li P, Rosen MK, Shen K. 2014. Local F-actin network links synapse formation and axon branching. Cell. 156:208–220.

Chisholm AD. 2013. Cytoskeletal dynamics in *Caenorhabditis elegans* axon regeneration. Annu Rev Cell Dev Biol. 29:271–297.

Chisholm AD, Hutter H, Jin Y, Wadsworth WG. 2016. The genetics of axon guidance and axon regeneration in *Caenorhabditis elegans*. Genetics. 204:849–882.

Choudhary B, Kamak M, Ratnakaran N, Kumar J, Awasthi A, *et al.* 2017. UNC-16/JIP3 regulates early events in synaptic vesicle protein trafficking via LRK-1/LRRK2 and AP complexes. PLoS Genet. 13:e1007100.

Clark SG, Chiu C. 2003. *C. elegans* ZAG-1, a Zn-finger-homeodomain protein, regulates axonal development and neuronal differentiation. Development. 130:3781–3794.

Ding C, Hammarlund M. 2018. Aberrant information transfer interferes with functional axon regeneration. Elife. 7:e38829.

Dogterom M, Koenderink GH. 2019. Actin-microtubule crosstalk in cell biology. Nat Rev Mol Cell Biol. 20:38–54.

Edwards SL, Yu SC, Hoover CM, Phillips BC, Richmond JE, *et al.* 2013. An organelle gatekeeper function for *Caenorhabditis elegans* UNC-16 (JIP3) at the axon initial segment. Genetics. 194:143–161.

El Bejjani R, Hammarlund M. 2012. Neural regeneration in *Caenorhabditis elegans*. Annu Rev Genet. 46:499–513.

Flynn KC, Hellal F, Neukirchen D, Jacob S, Tahirovic S, *et al.* 2012. ADF/cofilin-mediated actin retrograde flow directs neurite formation in the developing brain. Neuron. 76:1091–1107.

Ganguly A, Tang Y, Wang L, Ladt K, Loi J, *et al.* 2015. A dynamic formin-dependent deep F-actin network in axons. J Cell Biol. 210: 401–417.

Ghosh-Roy A, Goncharov A, Jin Y, Chisholm AD. 2012. Kinesin-13 and tubulin posttranslational modifications regulate microtubule growth in axon regeneration. Dev Cell. 23:716–728.

Ghosh-Roy A, Wu Z, Goncharov A, Jin Y, Chisholm AD. 2010. Calcium and cyclic AMP promote axonal regeneration in *Caenorhabditis elegans* and require DLK-1 kinase. J Neurosci. 30: 3175–3183.

Ghosh AS, Wang B, Pozniak CD, Chen M, Watts RJ, *et al.* 2011. DLK induces developmental neuronal degeneration via selective regulation of proapoptotic JNK activity. J Cell Biol. 194:751–764.

Gomez TM, Letourneau PC. 2014. Actin dynamics in growth cone motility and navigation. J Neurochem. 129:221–234.

Hammarlund M, Nix P, Hauth L, Jorgensen EM, Bastiani M. 2009. Axon regeneration requires a conserved MAP kinase pathway. Science. 323:802–806.

Hanz S, Perlson E, Willis D, Zheng JQ, Massarwa R, *et al.* 2003. Axoplasmic importins enable retrograde injury signaling in lesioned nerve. Neuron. 40:1095–1104.

He Z, Jin Y. 2016. Intrinsic control of axon regeneration. Neuron. 90: 437–451.

Holland SM, Collura KM, Ketschek A, Noma K, Ferguson TA, *et al.* 2016. Palmitoylation controls DLK localization, interactions and activity to ensure effective axonal injury signaling. Proc Natl Acad Sci USA. 113:763–768.

Hsu CH, Chan D, Wolozin B. 2010. LRRK2 and the stress response: interaction with MKKs and JNK-interacting proteins. Neurodegener Dis. 7:68–75.

Hubert T, Wu Z, Chisholm AD, Jin Y. 2014. S6 kinase inhibits intrinsic axon regeneration capacity via AMP kinase in *Caenorhabditis elegans*. J Neurosci. 34:758–763.

Hur EM, Saijilafu FQ., Zhou 2012. Growing the growth cone: remodeling the cytoskeleton to promote axon regeneration. Trends Neurosci. 35:164–174.

Hur EM, Yang IH, Kim DH, Byun Saijilafu J, Xu WL, *et al.* 2011. Engineering neuronal growth cones to promote axon regeneration over inhibitory molecules. Proc Natl Acad Sci USA. 108:5057–5062.

Ito M, Yoshioka K, Akechi M, Yamashita S, Takamatsu N, *et al.* 1999. JSAP1, a novel jun N-terminal protein kinase (JNK)-binding protein that functions as a scaffold factor in the JNK signaling pathway. Mol Cell Biol. 19:7539–7548.

Itoh A, Horiuchi M, Bannerman P, Pleasure D, Itoh T. 2009. Impaired regenerative response of primary sensory neurons in ZPK/DLK gene-trap mice. Biochem Biophys Res Commun. 383:258–262.

Kawasaki M, Hisamoto N, Iino Y, Yamamoto M, Ninomiya-Tsuji J, *et al.* 1999. A *Caenorhabditis elegans* JNK signal transduction pathway regulates coordinated movement via type-D GABAergic motor neurons. EMBO J. 18:3604–3615.

Kelkar N, Gupta S, Dickens M, Davis RJ. 2000. Interaction of a mitogen-activated protein kinase signaling module with the neuronal protein JIP3. Mol Cell Biol. 20:1030–1043.

Kim KW, Tang NH, Piggott CA, Andrusiak MG, Park S, *et al.* 2018. Expanded genetic screening in *Caenorhabditis elegans* identifies new regulators and an inhibitory role for NAD(+) in axon regeneration. Elife. 7:e39756.

Koushika SP, Schaefer AM, Vincent R, Willis JH, Bowerman B, *et al.* 2004. Mutations in *Caenorhabditis elegans* cytoplasmic dynein components reveal specificity of neuronal retrograde cargo. J Neurosci. 24:3907–3916.

Kyriakis JM, Avruch J. 2012. Mammalian MAPK signal transduction pathways activated by stress and inflammation: a 10-year update. Physiol Rev. 92:689–737.

Lee SI, Zhang W, Ravi M, Weschenfelder M, Bastmeyer M, *et al.* 2013. Atypical protein kinase C and Par3 are required for proteoglycan-induced axon growth inhibition. J Neurosci. 33: 2541–2554.

Li C, Hisamoto N, Matsumoto K. 2015. Axon regeneration is regulated by Ets-C/EBP transcription complexes generated by activation of the cAMP/Ca^{2+} signaling pathways. PLoS Genet. 11:e1005603.

Lindwall C, Kanje M. 2005. Retrograde axonal transport of JNK signaling molecules influence injury induced nuclear changes in p-c-Jun and ATF3 in adult rat sensory neurons. Mol Cell Neurosci. 29:269–282.

Lu W, Lakonishok M, Gelfand VI. 2015. Kinesin-1-powered microtubule sliding initiates axonal regeneration in *Drosophila* cultured neurons. Mol Biol Cell. 26:1296–1307.

Nakata K, Abrams B, Grill B, Goncharov A, Huang X, *et al.* 2005. Regulation of a DLK-1 and p38 MAP kinase pathway by the ubiquitin ligase RPM-1 is required for presynaptic development. Cell. 120:407–420.

Neumann B, Nguyen KC, Hall DH, Ben-Yakar A, Hilliard MA. 2011. Axonal regeneration proceeds through specific axonal fusion in transected *C. elegans* neurons. Dev Dyn. 240:1365–1372.

Nihalani D, Merritt S, Holzman LB. 2000. Identification of structural and functional domains in mixed lineage kinase dual leucine zipper-bearing kinase required for complex formation and stress-activated protein kinase activation. J Biol Chem. 275: 7273–7279.

Nihalani D, Wong HN, Holzman LB. 2003. Recruitment of JNK to JIP1 and JNK-dependent JIP1 phosphorylation regulates JNK module dynamics and activation. J Biol Chem. 278:28694–28702.

Nix P, Hammarlund M, Hauth L, Lachnit M, Jorgensen EM, *et al.* 2014. Axon regeneration genes identified by RNAi screening in *C. elegans*. J Neurosci. 34:629–645.

Nix P, Hisamoto N, Matsumoto K, Bastiani M. 2011. Axon regeneration requires coordinate activation of p38 and JNK MAPK pathways. Proc Natl Acad Sci USA. 108:10738–10743.

Noblett N, Wu Z, Ding ZH, Park S, Roenspies T, *et al.* 2019. DIP-2 suppresses ectopic neurite sprouting and axonal regeneration in mature neurons. J Cell Biol. 218:125–133.

Patel N, Thierry-Mieg D, Mancillas JR. 1993. Cloning by insertional mutagenesis of a cDNA encoding *Caenorhabditis elegans* kinesin heavy chain. Proc Natl Acad Sci USA. 90:9181–9185.

Rao GN, Kulkarni SS, Koushika SP, Rau KR. 2008. *In vivo* nanosecond laser axotomy: cavitation dynamics and vesicle transport. Opt Express. 16:9884–9894.

Sakamoto R, Byrd DT, Brown HM, Hisamoto N, Matsumoto K, *et al.* 2005. The *Caenorhabditis elegans* UNC-14 RUN domain protein binds to the kinesin-1 and UNC-16 complex and regulates synaptic vesicle localization. Mol Biol Cell. 16:483–496.

Schindelin J, Arganda-Carreras I, Frise E, Kaynig V, Longair M, *et al.* 2012. Fiji: an open-source platform for biological-image analysis. Nat Methods. 9:676–682.

Shin JE, Cho Y, Beirowski B, Milbrandt J, Cavalli V, *et al.* 2012. Dual leucine zipper kinase is required for retrograde injury signaling and axonal regeneration. Neuron. 74:1015–1022.

Sood P, Murthy K, Kumar V, Nonet ML, Menon GI, *et al.* 2018. Cargo crowding at actin-rich regions along axons causes local traffic jams. Traffic. 19:166–181.

Stone MC, Nguyen MM, Tao J, Allender DL, Rolls MM. 2010. Global up-regulation of microtubule dynamics and polarity reversal during regeneration of an axon from a dendrite. Mol Biol Cell. 21: 767–777.

Sun F, Zhu C, Dixit R, Cavalli V. 2011. Sunday Driver/JIP3 binds kinesin heavy chain directly and enhances its motility. EMBO J. 30: 3416–3429.

Tang NH, Chisholm AD. 2016. Regulation of microtubule dynamics in axon regeneration: insights from *C. elegans*. F1000Res. 5: 764.

Tedeschi A, Dupraz S, Curcio M, Laskowski CJ, Schaffran B, *et al.* 2019. ADF/Cofilin-mediated actin turnover promotes axon regeneration in the adult CNS. Neuron. 103:1073–1085.e6.

Trent C, Tsuing N, Horvitz HR. 1983. Egg-laying defective mutants of the nematode *Caenorhabditis elegans*. Genetics. 104:619–647.

Valakh V, Frey E, Babetto E, Walker LJ, DiAntonio A. 2015. Cytoskeletal disruption activates the DLK/JNK pathway, which promotes axonal regeneration and mimics a preconditioning injury. Neurobiol Dis. 77:13–25.

Verhey KJ, Meyer D, Deehan R, Blenis J, Schnapp BJ, *et al.* 2001. Cargo of kinesin identified as JIP scaffolding proteins and associated signaling molecules. J Cell Biol. 152:959–970.

Villanueva A, Lozano J, Morales A, Lin X, Deng X, *et al.* 2001. *jkk-1* and *mek-1* regulate body movement coordination and response to heavy metals through *jnk-1* in *Caenorhabditis elegans*. EMBO J. 20:5114–5128.

Wang Z, Jin Y. 2011. Genetic dissection of axon regeneration. Curr Opin Neurobiol. 21:189–196.

Watt D, Dixit R, Cavalli V. 2015. JIP3 activates Kinesin-1 motility to promote axon elongation. J Biol Chem. 290:15512–15525.

Whitmarsh AJ. 2006. The JIP family of MAPK scaffold proteins. Biochem Soc Trans. 34:828–832.

Whitmarsh AJ, Cavanagh J, Tournier C, Yasuda J, Davis RJ. 1998. A mammalian scaffold complex that selectively mediates MAP kinase activation. Science. 281:1671–1674.

Wu Z, Ghosh-Roy A, Yanik MF, Zhang JZ, Jin Y, *et al.* 2007. *Caenorhabditis elegans* neuronal regeneration is influenced by life stage, ephrin signaling, and synaptic branching. Proc Natl Acad Sci USA. 104:15132–15137.

Xiong X, Collins CA. 2012. A conditioning lesion protects axons from degeneration via the Wallenda/DLK MAP kinase signaling cascade. J Neurosci. 32:610–615.

Xiong X, Wang X, Ewanek R, Bhat P, Diantonio A, *et al.* 2010. Protein turnover of the Wallenda/DLK kinase regulates a retrograde response to axonal injury. J Cell Biol. 191:211–223.

Yamamoto N, Hegde AN, Chain DG, Schwartz JH. 1999. Activation and degradation of the transcription factor C/EBP during long-term facilitation in *Aplysia*. J Neurochem. 73:2415–2423.

Yan D, Jin Y. 2012. Regulation of DLK-1 kinase activity by calcium-mediated dissociation from an inhibitory isoform. Neuron. 76:534–548.

Yan D, Wu Z, Chisholm AD, Jin Y. 2009. The DLK-1 kinase promotes mRNA stability and local translation in *C. elegans* synapses and axon regeneration. Cell. 138:1005–1018.

Yanik MF, Cinar H, Cinar HN, Chisholm AD, Jin Y, *et al.* 2004. Neurosurgery: functional regeneration after laser axotomy. Nature. 432:822.

Zeke A, Misheva M, Reményi A, Bogoyevitch MA. 2016. JNK signaling: regulation and functions based on complex protein-protein partnerships. Microbiol Mol Biol Rev. 80:793–835.

Zou Y, Chiu H, Zinovyeva A, Ambros V, Chuang CF, *et al.* 2013. Developmental decline in neuronal regeneration by the progressive change of two intrinsic timers. Science. 340:372–376.

Communicating editor: B. Grant